



ЕЛЕКТРОТЕХНИЧКИ ФАКУЛТЕТ  
УНИВЕРЗИТЕТА У БАЊАЛУЦИ

---

*FACULTY OF ELECTRICAL ENGINEERING  
UNIVERSITY OF BANJALUKA*

# ЕЛЕКТРОНИКА

# *ELECTRONICS*

**YU ISSN 1450-5843**

ГОДИШТЕ 6, БРОЈ 1, ДЕЦЕМБАР 2002. *VOLUME 6, NUMBER 1, DECEMBER 2002.*

## FACULTY OF ELECTRICAL ENGINEERING UNIVERSITY OF BANJALUKA

Address: Patre 5, 78000 Banjaluka, Republic of Srpska, Bosnia and Herzegovina  
Phone: + 387 51 211-408, + 387 51 221-820  
Fax: + 387 51 211-408

## ELECTRONICS

e-mail: [elektronika@etfbl.net](mailto:elektronika@etfbl.net)

*Editor:* Prof. Branko L. Dokić, Ph. D.  
Faculty of Electrical Engineering  
University of Banjaluka, Republic of Srpska  
e-mail: [bdokic@etfbl.net](mailto:bdokic@etfbl.net)

### *Program Committee:*

- Nikolaos Uzunoglu, National Technical University of Athens, Greece
- Barry Jefferies, University of Hertfordshire, UK
- Vojin Oklobdžija, University of California, Davis, USA
- Bratislav Milovanović, Faculty of Electronics Niš, FR Yugoslavia
- Milić Stojić, Faculty of Electrical Engineering Beograd, FR Yugoslavia
- Vojislav Arandelović, Institute "Vinča" Beograd, FR Yugoslavia
- Veljko Milutinović, Faculty of Electrical Engineering Beograd, FR Yugoslavia
- Ilija Stojanović, SANU Beograd, FR Yugoslavia
- Vladimir Katić, Faculty of Technical Sciences Novi Sad, FR Yugoslavia
- Aleksandar Ilišković, Faculty of Electrical Engineering Banjaluka, RS
- Milorad Božić, Faculty of Electrical Engineering Banjaluka, RS

*Secretary:* Petar Matić, M.Sc.  
e-mail: [pero@etfbl.net](mailto:pero@etfbl.net),  
Faculty of Electrical Engineering  
University of Banjaluka, Republic of Srpska

*Publisher:* Faculty of Electrical Engineering  
University of Banjaluka, Republic of Srpska  
Address: Patre 5, 78000 Banjaluka, Republic of Srpska, Bosnia and Herzegovina  
Phone: + 387 51 211-408, + 387 51 221-820  
Fax: + 387 51 211-408  
<http://www.etfbl.net>

## PREFACE

The 46<sup>th</sup> Conference on Electronics, Telecommunications, Computer Sciences, Automation, and Nuclear Technique (ETRAN 2002) was held on June 4-7 in Banja Vrućica – Teslić. This year's ETRAN Conference was held in the Republic of Srpska on the occasion of 40<sup>th</sup> Anniversary of the Faculty of Electrical Engineering Banja Luka. The conference was, for the first time, organized in cooperation with IEEE Yugoslavia Section.

This year's issue of the most outstanding national conference in the field has maintained its high level in respect to the number of participants (over 500) and quality of papers presented. The total of 299 papers have been presented within 16 technical sessions: Electronics (EL), Telecommunications (TE), Computer Technique (RT), Automation (AU), Nuclear Technique and Technologies (NT), Acoustics (AK), Antennas and Propagation (AP), Artificial Intelligence (VI), Electrical Circuits and Systems & Signal Processing (EK), Electroenergetics, Biomedical Technique (ME), Metrology (ML), Microelectronics and Optoelectronics (MO), Microwave and Submillimeter Technique (MT), New Materials (NM), and Robotics and Flexible Automation (RO). The number of papers presented at each session was as follows: TE 34, MO 34, RT 27, ME 21, EL 20, AU 19, EE 19, AP 17, ML 17, MT 17, AK 16, NM 16, NT 15, EK 14, VI 7, RO 7. A particular feature of this conference issue was participation of a number of young researchers from both academia and industry coming from Serbia, Montenegro and Republic of Srpska.

As in earlier issues, there was a Plenary Session, this time devoted to the developments of telecommunications, with three invited papers: "Guidelines for the policy of telecommunication sector of Republic Srpska" (Prof. Dr. Branko Dokić), "New services – the strategic orientation of Telecom Srpska" (Mr. Željko Jungić), and "Development of telecommunication systems in Serbia and neighbouring countries" (Prof. Dr. Djordje Paunović). The round tables entitled "Reformation of education in electrical engineering" and "Equal access to information-communication technologies (ICT)" were also held. Participants have shown a special interest in the round table on reformation of education, at which Prof. Dr. Kurt Richter, IEEE Education Committee Member, and Prof. Dr. Srbijanka Turajlić, Serbian Deputy Minister of Education and Sport, gave their introductory talks.

This year the Best Paper Awards for young researchers were introduced, and 11 technical session committees (EL, AU, AK, AP, VI, EE, EK, ML, MO, MT, NM) presented these awards at the conference closing. This special issue contains the updated versions of 10 awarded papers. Interested readers will find that the quality and practical value of these papers represent not only the current developments in the field in this geographic region but are also in line with the latest developments worldwide.

Prof. dr Branko Kovačević  
Chair, ETRAN Programme Committee

Prof. dr Ninoslav Stojadinović  
Chair, Society for ETRAN

### Biography of Prof. Dr. Ninoslav Stojadinovic



Ninoslav D. Stojadinovic was born in Nis, Yugoslavia, in 1950. He received the Dipl. Ing., M. Sc. and D. Sc. degrees, all in electrical engineering, at the Faculty of Electronic Engineering, University of Nis, in 1974, 1977 and 1980, respectively.

In 1974 he joined the Ei-Semiconductors, Nis, where he worked in R&D of bipolar semiconductor devices, such as low-voltage Zener diodes, hyper-abrupt varicap diodes and planar bipolar transistors. In 1976, he joined the Faculty of Electronic Engineering, University of Nis, where he is now Professor of Microelectronics and Head of the Department of Microelectronics. His current research interest involves various aspects of MOS devices and circuits, ranging from device physics and modeling, process and device simulation, and characterization and reliability. He is distinguished lecturer of the IEEE Electron Devices Society for the area of microelectronics reliability. He is author or coauthor of over 60 papers published in refereed international journals and 120 papers presented at international and national conferences. He was supervisor of more than 40 Dipl. Ing. thesis, 10 M.Sc thesis and 11 D. Sc. thesis in the field of microelectronics.

Dr. Stojadinovic is Editor-in-Chief of Microelectronics Reliability journal and Editor-in-Chief of IEEE Electron Devices Society Newsletter. He is also the Programme Committee Chairman of the IEEE International Conference on Microelectronics (MIEL). He is Chair of Yugoslavia IEEE Section and Yugoslavia ED/SSC Chapter, President of the Society for ETRAN, and member of Yugoslav Academy of Engineering.

### Biography of Prof. Dr. Branko Kovacevic



Branko D. Kovačević was born in Belgrade, Yugoslavia on 29 June, 1951. He received the B.Sc., M.Sc., and Ph.D. degrees from the University of Belgrade in 1975, 1980, and 1984, respectively. From 1975 to 1977 he was a research associate in the Computer Science Laboratory, Institute Mihailo Pupin, Belgrade. From 1977 to 1981 he was a research fellow in the Department of Automatic Control, Military Institute of Technology, Belgrade. In 1981 he joined the Faculty of Electrical Engineering, University of Belgrade, where he is presently Full Professor, teaching courses in control systems theory and its applications. He was awarded the Engineers Prize of the Economic Council of Belgrade, The Dušan Mitrović Prize of the Yugoslav Society of Electrical Engineers (ETRAN), the Branko Raković Prize of the Faculty of Electrical Engineering, the Outstanding Research Prize of the Institute of Applied Mathematics and Electronics, and the Teaching Prize of the University Students Council. He is also a member of IEEE, a member of EURASIP, a member of ETRAN, the President of ETRAN Section for Automatic Control, the President of ETRAN Program committee and the Editor in chief of the Journal of Automatic Control (published by the Belgrade University Press). Dr. Kovačević was also a visiting professor at the Florida State University, as well as a lecturer at the European Institute for System Sciences. Dr. Kovačević is author of eight books and over 90 scientific journal papers and 200 conference papers. He was also the supervisor of nearly 100 Diploma engineering thesis, 40 M.Sc. thesis and 10 Ph.D. thesis. His research interests lie in the field of estimation, system identification, adaptive control and digital signal processing.

## DESIGN OF PRINTED CIRCUIT BOARDS FOR LOW-POWER RADIO TRANSMITTERS

Miljana Sokolović, Dragiša Milovanović, Faculty of Electronic Engineering, Niš

**Abstract:** For RF designers developing low-power radio devices for short-range applications, antenna design has become an important issue for the total radio system design. Having in mind the demand for small size and low cost in the development of such radio modules, a small-tuned loop antenna on the same printed circuit board as the radio module is a good and practical solution. In order to achieve good results, designer has to keep in mind how the antenna and the transmission module work. Some suggestions for efficient design of printed circuit boards and antennas for low-power RF radio transmitters have been proposed in this paper

### 1. INTRODUCTION

With the advent of science and technology, a need evolved to a modern man to have everything on the reach of his hand. This was specially regarded to the electronic devices and means of communication. For this kind of devices, it is not just important to be mobile that is wireless, but to have small dimensions, low power consumption and to be immune of environmental influences. Very large number and variety of these devices brought up to the increase of their working frequencies. In that way we came up to that the most often used frequencies are from RF frequency range. However, with the increase of frequencies some difficulties in maintaining good performances of those systems appear. Some parasitic effects and other external influences significantly degrade performances of electronic devices.

On the other hand, mobile devices should be small enough and compact also. They should not be significantly influenced by the external changes (for example the influence of the user's hand and his body, or the shape and the type of the package, and the material it is made of). Also, during the design of these devices one should have in mind the simpler and more accurate solution for frequency adjustment.

In the following sections the working principle will be given of one transmitter circuit having digital input signal, later processed and applied to one compact printed loop antenna. After this, some dimension calculations for printed loop antennas will be presented for achieving a required frequency range. It will be explained latter the process for layout design of that module, using a tool for designing printed circuit board PCAD. During that some important recommendation will be given that should be kept in mind while designing those modules. Paying attention to these issues leads to:

- better antenna radiation, avoiding use of external antenna,
- better matching of antenna to the transmitter circuit,
- less parasitic effects caused by the printed board itself,
- less environment influence.

Measurement results of the manufactured board and the conclusion will be presented at the end of this paper.

### 2. ANTENNA'S TRANSMITTER IC

The circuit that will be described next is used in systems such as:

- alarm and security systems
- keyless car and central locking
- low-power telemetry systems
- general digital data transmission
- general analog audio signal transmission
- local oscillator signal generation
- systems for wireless data transfer
- remote control systems
- fire protection systems

Transmitter circuit uses ready-made integrated transmitters [1]. Block diagram of this IC is shown in Figure 1. This IC receives the digital signal, processes it and performs amplitude modulation (ASK) in order to get the signal waveform appropriate for antenna feeding. Transmitter IC-s are available in two versions: differential output and single ended output. An integrated transmitter circuits with a differential output will be used here to emphasis the bad influence of asymmetry to the antenna and the whole circuitry.

In order to get a full picture, some basic characteristics of this IC will be given next [2].

Figure 1 shows the transmitter circuit that consists of a fully integrated voltage controlled oscillator (VCO), a divide-by-32 divider ( $N=32$ ), a phase-frequency detector (PFD) and a charge pump circuit. External loop filter determines the dynamic behavior of the PLL (Phase Locked Loop) and suppresses reference spurious signals.

The output of VCO drives the power amplifier (PA). RF output power  $P_o$  can be adjusted to have one of four predefined output power steps in the range -15dBm to +1dBm. The adjustment can be performed by changing the value of external resistor  $R_{F1}$ , or by changing the value of  $V_{PS}$  voltage at the control pin PS/DATA. The differential output is realized as an output with an open collector, and can be used for direct loop antenna feeding. In order to reach the maximum output power, the differential output should be matched with an input impedance of the load having resistance about  $1k\Omega$ . Integrated circuit operates stable in the supply voltage range from 2,2V to 5,5V.

This circuit can perform ASK modulation in that way that data stream is applied directly at the PS-pin. This turns the internal current sources of the power amplifier on and off and therefore forwards an ASK signal to the output.

Many applications need a stable RF source. Regarding to that, this circuit can function without performing the modulation, just like a simple PLL stabilized generator of continuous signal.

If needed, the circuit can perform a FM modulation, and then an external variable capacitor is required. It simply works as a pulling resistor that is in series connected to the crystal. Then, the analog modulation signal, going through a series connected resistor directly modulates the signal applied at XOSC pin.

series connected resistor directly modulates the signal applied at XOSC pin.

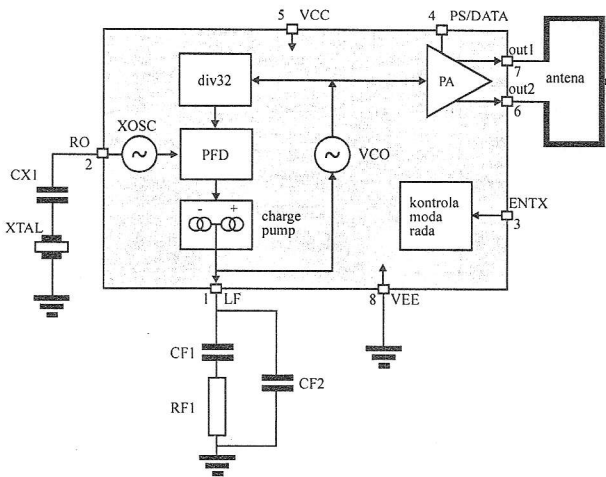


Fig. 1: Block diagram of transmitter IC

The mode control logic has two different operating modes. The mode control pins are pulled-down internally. This guarantees that the whole circuit is shut down if these pins are left floating.

3. ANTENNA EVALUATION

Let us consider now the computations for antenna design. This antenna is connected at the output of the amplifier. Its dimensions are determined by the working frequency of the device [3]. Since the whole integrated circuit is designed to give the best results while working in a frequency range from 310MHz to 480MHz, that is from 800MHz to 930MHz, this fact has to be taken into account in antenna computation and design.

The antenna has a rectangular shape and two access points. The thickness of antenna's copper trace is the same as the thickness of the lines and connections on the printed circuit board (PCB). This means that the antenna is realized in the same fabrication step as lines and connections on the same printed circuit board. For it's fabrication there are no additional money expenses and time consumptions. Just some more material is needed (which is also negligibly small), that is copper and epoxy glass.

Figure 2, shows the shape of the antenna with dimensions of interest.

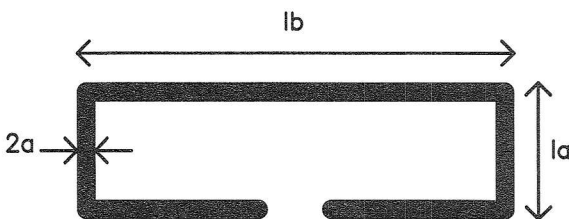


Fig. 2: The shape of printed loop antenna

The surface of the antenna is calculated as follows:  $A = l_a \times l_b$ . It is extremely important that during the antenna design the next relation between dimensions is maintained:  $l_a, l_b \gg 2a$ .

Impedance of small printed loop antenna can be derived using the corresponding equivalent circuit. Since the antenna itself is just one copper loop, though the equivalent circuit for it will be a series connection of radiation resistance, equivalent loss resistance in the copper and the inductance of the loop. Equivalent circuit is shown in the figure 3.

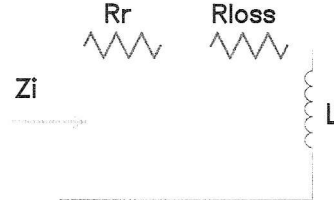


Fig. 3: Equivalent electrical circuit of printed loop antenna

The impedance of a small loop antenna can be expressed equivalently by using circuit parameters as shown in the figure 3:

$$Z_i = R_r + R_{loss} + j\omega L \tag{1}$$

where  $R_r$  denotes the radiation resistance,  $R_{loss}$  loss resistance and  $L$  self-inductance of the loop structure. The radiation resistance can be determined from [3]:

$$R_r = 20(\beta^2 A)^2, \tag{2}$$

where we have  $\beta = 2\pi/\lambda$  and  $A = l_a \times l_b$ .

Loss resistance can be calculated as follows:

$$R_{loss} = \frac{1}{2\pi}(l_a + l_b)R_s, \text{ where is } R_s = \sqrt{\frac{\pi f \mu_0}{\sigma}}, \tag{3}$$

and  $\sigma$  is the conductance of the copper.

Inductivity of the structure can be determined in the following way:

$$L = \frac{\mu_0}{\pi} \left[ l_b \ln \left\{ \frac{2A}{a(l_b + l_c)} \right\} + l_a \ln \left\{ \frac{2A}{a(l_a + l_c)} \right\} + 2\{a + l_c - (l_a + l_b)\} \right] \tag{4}$$

where is  $l_c = \sqrt{l_a^2 + l_b^2}$

The efficiency of the antenna is expressed as the ratio of the power of the antenna's input signal, and the power of the antenna' radiation. For this type of the antenna, the efficiency is given by:

$$\eta = \frac{R_r}{R_r + R_{loss}}. \tag{5}$$

Antenna gain is measure of how strongly the antenna radiates comparing to a reference antenna, such as a dipole. It can be computed as:

$$G_L = G_D \cdot \eta \cdot \gamma. \tag{6}$$

$G_D$  stands for the directive gain with respect to the standard half-wave dipole,  $\eta$  is antenna efficiency, and  $\gamma$  is the mismatch factor. Just like all compact antennas, this also have poor gain. According to the calculated values for input admittance, its resonant frequency can be determined. Parallel with access points of the antenna, one capacitor can be connected to tune and match the antenna contributing the resonance establishing.

Computations of the antenna dimensions gave the following values:

During the calculation it is considered that the copper trace width is  $2a = 2mm$ , and its thickness is standard  $0,034mm$ .

#### 4. DESIGN OF PRINTED CIRCUIT BOARDS USING PCAD TOOL

Integrated circuit described above and the antenna, are the major parts of the transmitter circuit board. They should now be carefully connected with the other circuitry components. PCAD tool makes this step very simple. PCAD consists of many tools. The most important for this step are Schematic editor and PCB Layout editor. Design of double-sided printed circuit boards has few steps. First it is necessary to create a schematic of the whole circuit using the Schematic editor. Then we move to the PCB Layout editor where we have to set up the workspace, just like in any other CAD (Computer Aided Design). During this step following things can be set up: workspace, display control, layers, line width, pads and via stacks, grids, libraries, and board dimensions. After that, net-list of the whole circuit, which was already created in Schematic editor, is exported into PCB Layout editor. While doing this every symbol from the Schematic editor is automatically replaced by its footprint in the PCB. For this design step values of the elements (such as resistance or capacity) are not of interest, but just their footprints, that is the dimensions and the arrangement of their pins, packages and pads. Now it is necessary to do the placement of all components on the board. Next step is routing the connections between the components. This step can be performed in two ways: automatically or manually. Since the lines length is very critical for this step, and since the board does not consist of a lot of components, than it is more convenient to perform this step manually and not automatically. The antenna is formed in the same manner like lines and connections on the board, though it is done in the same fabrication step. When components are placed and connected areas of copper should be laid down on the top and the bottom side of the board with a back-off from tracks and pads within the area. These layers insure good grounding. Placement, traces routing and copper pouring should be done with a respect to a certain design rules. Some of these rules will be mentioned below. Figure 4 shows layouts of designed printed circuit boards for two different working frequencies with an appropriate dimensions marking.

In order to bring up the design to the end successfully, it is necessary to verify the design. After this step it can be said if the whole circuit is designed well or bad. Verification is done in two phases:

1. Design rule check. Concrete design solutions are checked regarding to physical and electrical limitations.
2. Net-list verification. During this step a comparison of net-list extracted from the layout and imported from the schematic is performed, and one can come to the conclusion that all necessary elements and connections are present on the final board design.

The last step of design is generating the files needed for controlling the fabrication process [5]. The N/C Drill file controls precise drillers used for making pins, via holes etc, should be generated next. One more file (Gerber file) controls machines for creating layers on the board.

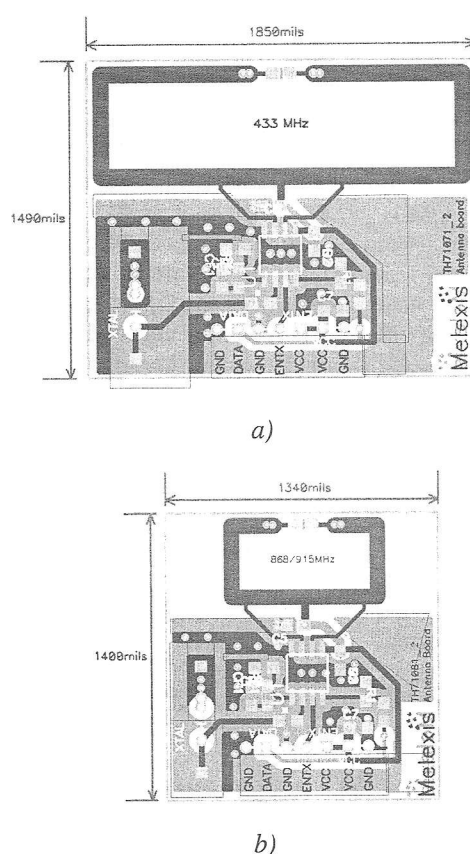


Fig. 4: Layout of the printed antenna transmitter: a) the frequency is 433MHz, b) the frequency is 866MHz

#### 5. SPECIAL ISSUES CONSIDERED IN ANTENNA RF CIRCUITRY LAYOUT DESIGN

In order to achieve good performances of RF antenna transmission devices it is important to pay a special attention to some issues. These issues do not have to be respected if the working frequencies of systems are not very high. However, with the increase of the working frequency some parasitic effect can significantly change the circuit behavior.

Requirements that should be respected here can be classified into few groups. First group of specific issues deals with a grounding process. Second group stands for special issues in the component placement and lines tracing. The third group is for the special issues of the power lines realization. The last group, but not less important, considers improving the antenna performances.

Regarding to the special issues of grounding process, ground layer (usually placed on the bottom side of the board) should not have many cut-offs. Because of that, lines on the bottom side should be avoided. If they are necessary, they should be made as short as possible. The reason for this lies in the fact that good grounding is very important for high working frequencies modules. Since the top side of the board also has some grounding areas, and since the board can have just one ground potential, though it is necessary to have as many via holes between the top and the bottom grounding areas as possible in order to equalize their potentials. For some groups of elements it is also important to isolate their ground connections in order to reduce the influence of their signals to the signals of the other groups of elements. It

just one ground potential, though it is necessary to have as many via holes between the top and the bottom grounding areas as possible in order to equalize their potentials. For some groups of elements it is also important to isolate their ground connections in order to reduce the influence of their signals to the signals of the other groups of elements. It means that some ground areas on the top side of the board should be isolated from the rest of the circuit. Regarding to the shape of these areas sharp angles should be also avoided. These structures are the places for charge accumulating, and it is better to cut them off or at least to make some roundness.

Regarding to the component placing and lines tracing, some attention should be paid that these lines are traced as short and close as possible, but not to much because of the additional parasitic effects (which can form a virtual components in the circuit). Large current lines should be proportionally wider. Lines with the digital signals should be as far as possible from the analog signal lines. The same case stands for lines with input and output signals. They should also not be intersected.

It is important for power supply lines to be wide enough in order to have the same potential at all their points. It is also important that these lines do not form a loop on the board structure. The supply should be applied at more than one point of the circuit. This can be performed using the buss or the star topology.

Regarding to the antenna, it should be placed on the top side of the board and as far as possible from the rest of the circuitry and from the ground plane. Ground areas are made of metal (copper) and they are behaving like reflectors. Tracing lines and text near the antenna structure should be also avoided. Additional text and marks on the board are also made as the other lines. In order to avoid asymmetry in the frequency spectrum, antenna and the rest of the board should have a certain extent of symmetry. This is specially regarding to the grounding layers. There are also different solutions of antenna biasing that can contribute to the better antenna radiation.

## 6. MEASUREMENT RESULTS

After the final board is manufactured, and all elements are soldered on it, some measurements should be performed. Obtaining characteristics of the board can be performed using a spectrum analyzer. Frequency spectrum for the board shown in figure 4a that was the result of measurement is shown in figure 5. Just a result of the measurement for the transmitter board for the 433MHz working frequency is shown here. The figure presents a frequency dependence of the transmitter circuit output power. Similar result can be expected for the board with 866MHz working frequency.

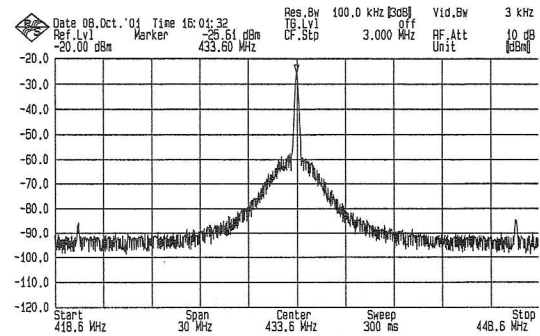


Fig. 5: Frequency spectrum shown on the spectrum analyzer

## 7. PACKAGE SELECTION

Also important influence to the whole antenna transmission system operating has its package and the environment. During the package selection one should keep in mind that every metal surface obstructs the antenna radiation. Metal surfaces are reflectors for antenna's radiated electro-magnetic waves. Concerning to that, if some metal parts of the package cannot be omitted, their dimensions should be kept as small as possible and out of reach of the antenna board.

It should be mentioned that antenna radiation could depend on the environment where the system is used. Also during the measurements an attention should be paid to the presents of some other devices in the close surroundings. Also if they cannot be omitted, they should be maintained equal for each measurement. These can be some other measurement systems and persons that do the measurement.

## 8. CONCLUSION

In the design process of printed RF transmitter circuit, antenna should be considered as an element that has a critical influence to the whole circuit performances. Most important antenna's characteristics its efficiency and its low cost. Some practical advices for achieving better and more efficient antenna transmitter module design are proposed in this paper. The results of a practical work are shown here. Antenna boards that have been presented here are used in the remote control systems, central locking systems and other system that are fabricated in the Melexis company, Germany.

## 9. REFERENCES

- [1] "Small loop antennas" Nord IC VLSI ASA, Application note, Norway, February 2000.
- [2] www.melexis.com
- [3] Kent Smith "Antennas for low power application", RF Monolithics, Dallas, December 2000.
- [4] -, "PCAD 2000 specialized design tools for PCB professionals; PCB Design", ACCEL Technologies, Inc,
- [5] M. Flatt, "Printed circuit boards basics; an introduction to the PCB industry", published by IPC, Manhattan, January 1997.

## A CONCATENATIVE TTS SYSTEM IN SERBIAN LANGUAGE BASED ON REAL-TIME SELECTION OF SEGMENTS

*Milan Sečujski, Radovan Obradović, Darko Pekar, Ljubomir Jovanov, School of Engineering, University of Novi Sad, Yugoslavia*

**Abstract:** *This paper presents some basic criteria for conception of a concatenative text-to-speech synthesizer in Serbian language. The paper describes the prosody generator which was used, and reflects upon several peculiarities of Serbian language which led to its adoption. The paper also describes criteria for on-line selection of appropriate segments from a large speech corpus.*

**Keywords:** *Text-to-Speech, Real-Time Segment Selection*

### 1. INTRODUCTION

Being a very prospective speech technology, speech synthesis has been thoroughly studied at the University of Novi Sad, Yugoslavia, within the AlfaNum project, for several years. One of the main goals of this project is the design of a high-quality concatenation-based speech synthesizer for Serbian language. The first version of the AlfaNum synthesizer is based on TD-PSOLA algorithm, performed on segments selected on-line from a large speech database containing continuous speech, according to various criteria defined beforehand. This paper gives a detailed description of the AlfaNum synthesizer, including descriptions of a dictionary-based prosody generation module, and implementation of on-line selection of segments. Off-line preprocessing of the speech corpus which was necessary for implementation of TD-PSOLA algorithm is also described.

### 2. ON SOME PECULIARITIES OF SERBIAN LANGUAGE

In this paper we will discuss some peculiarities of Serbian language that are relevant for speech synthesis. There are several important aspects in speech synthesis where those peculiarities should be taken into account.

One of the most remarkable features of Serbian language is its most simple grapheme-to-phoneme conversion rule. Namely, each letter corresponds to exactly one sound. The exceptions to this rule are exceedingly rare and most of them can occur only at the boundaries between two words. Several phonemes have their allophones, but that has little effect on intelligibility. Thus, the task of phonetization in Serbian speech synthesis is reduced to a trivial check, and solutions based on dictionaries and morphophonemic rules are not needed.

The task of a prosody generator is to ensure that the pronounced phrase sounds as naturally as possible. Generally, beside being more agreeable to a human listener, natural-sounding synthesized speech is easier to understand inasmuch as it is easier to perform lexical segmentation upon it, that is, to identify boundaries between words. In Serbian language, the importance of natural prosody is even more emphasized, since the location of stress within words is sometimes an essential feature of the meaning of that word.

The five vowels of Serbian language can be stressed in four different ways each, according to pitch level during the stressed vowel itself, its relation to the pitch level of the next syllable, and duration of stressed syllable, which falls into two classes: long and short. Four different types of stress can thus be recognized as rise/long, rise/short, fall/long and fall/short, as shown in Figure 1. Depending on stress types, timbre of these vowels, as well as formant structure, can also vary. Due to difficulties in modifying vowel timbre without use of more computationally intensive parametric speech synthesis algorithms, and thus avoiding timbre mismatches that lower the quality of synthesized speech, the solution we adopted was defining classes of distinctive timbre variants of each vowel, and considering them as different vowels altogether. This must be taken into account not only when performing grapheme-to-phoneme conversion, but also when labeling the speech database.

### 3. THE SPEECH DATABASE

#### 3.1. The contents

The speech database contains approximately two hours of continuous speech, pronounced by a single female speaker. Having in mind possible applications of such a system, and the fact that concatenation of longer speech segments yields more intelligible speech, it was decided that the database should include phrases such as commonplace first and last names, addresses, names of companies, cities and countries, amounts of money, currencies, time and date phrases, weather reports, horoscope reports, typical phrases used in interactive voice-response systems, typical phrases used in e-mail messages etc. The database was recorded in laboratory conditions, and submitted to several off-line operations necessary for implementing TTS, such as labeling the database and its pitch-marking.

#### 3.2 Labeling and pitch-marking

The labeling of the database consists of placing boundaries between units belonging to a previously established set of units such as phonemes. It actually implies storing information about units in a separate database. The labeling of the AlfaNum speech database was predominantly phoneme based, although in some cases a better alternative was adopted, due to certain phonetic features of particular phones, as well as certain peculiarities of Serbian language. For instance, some classes of phones, such as plosives and affricates, were considered as pairs of semiphones (including occlusion and explosion in case of plosives and occlusion and friction in case of affricates). Vowels belonging to classes with significantly different timbres were considered as different vowels altogether, and therefore not interchangeable. Considering the way the phoneme R is pronounced in Serbian language (a periodical set of occlusions and explosions produced by the tongue oscillating against the hard palate), all of these occlusions and explosions were

identified. Beside unit boundaries, a part of each unit least affected by coarticulation was identified, in order to make further prosody modifications less audible. Since the database contains continuous speech abounding in phones impaired in various degrees, such cases were all noted including the

degree of impairment, in order to avoid using these phones in contexts where they are usually well-articulated, for instance, within stressed syllables. This refers to both vowels and consonants.

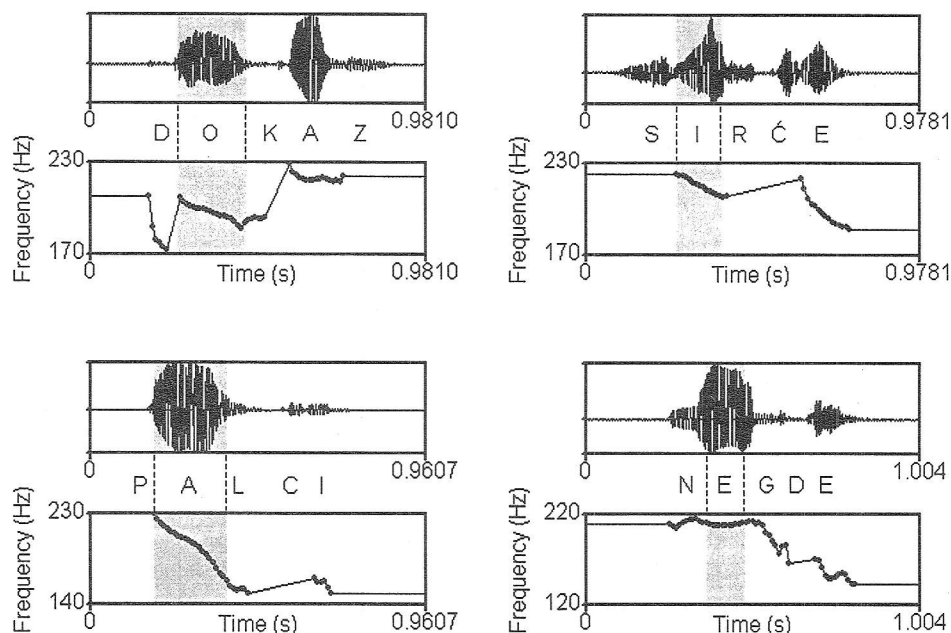


Figure 1. Stress types in Serbian language and corresponding pitch contours:

(a) rise/long, (b) rise/short, (c) fall/long, (d) fall/short, as pronounced

by the speaker involved in database recording. Labeling was performed automatically, using the AlfaNum continuous speech recognizer [7], and verified by a human expert. Verifying was based on signal waveform, its spectrogram and its auditory perception. The SpeechVis software, previously developed within the AlfaNum project, was used [8]

Implementing TD-PSOLA algorithm implies previous pitch-marking of the database, that is, detecting locations within phones most suitable for centering overlapping windows and extracting frames, in case a TTS algorithm which requires pitch-synchronous frame positioning should be used. Thus, during voiced frames, one marker per period was appointed, and during unvoiced frames, markers were appointed according to the average fundamental frequency throughout the database. In order to avoid audible effects caused by abrupt changes in V/UV marker positioning strategies, UV positioning strategy was somewhat modified in the vicinity of V/UV boundaries, and thus the rate with which distances between adjacent markers can vary was severely reduced.

As to positioning pitch markers within voiced frames, the process was carried out in two phases. To begin with, preliminary estimations of pitch contours of each segment were made using AMDF pitch-extraction method. Each of the segments was previously low pass filtered with  $f_c = 900$  Hz. The next step was locating the frame with the highest degree of voicing and locating the maximum peak within that frame. The initial pitch marker was placed there. Afterwards, the search for other pitch markers was conducted according to preliminary pitch estimations, which resulted in placing pitch markers in such a way that windows centered around them would cover most of the waveform's energy, and no

significant distortion of the signal caused by windowing could occur.

Such a procedure is not entirely error-free, because low pass filtering can sometimes modify peak values to such an extent that peaks recognized as maximum in some segments do not coincide with peaks recognized as maximum in the rest. This can happen in case of voiced phones whose waveforms have two prominent peaks of roughly the same height. There is another reason why errors of this kind may occur. At the precise spot of boundaries between phones there is sometimes an irregularity in functioning of the glottis, leading to a discontinuity in positions of glotal impulses. If a phoneme-based pitch-marking is adopted, that is, if pitch-marking is performed independently within phones, and not within speech segments containing more than one phone, most of such errors are eliminated completely.

The database containing information about pitch markers is suitable for speech synthesis using any of the concatenation-based techniques, even in case of techniques that do not require explicit knowledge of pitch markers, since pitch contours can be determined from pitch marker positions in a straightforward way.

word by word, in order to get information such as stress types and locations, part of speech classes and functions of particular words in the sentence. Grammatical information is essential for synthesis of natural-sounding prosody, since words in Serbian language can sometimes be stressed in different ways depending on their morphologic categories, and sometimes even have different meanings if stressed differently. In some cases even syntactic analysis does not help, and several interpretations of the same sentence, all of them grammatical, can be stressed in different ways and therefore yield different meanings. For a human listener there is no confusion, because he/she relies on contextual information.

#### 4.1. The dictionary

Since stress in Serbian language is fairly unpredictable, a dictionary-based solution was adopted, and described in detail in [6]. A special dictionary including information on stress configuration, part of speech class and morphologic categories for each word was created. The dictionary contains more than one million words, including inflected forms.

Such a solution is not entirely error-free, since it does not include syntactic analysis, nor does it solve cases when syntactic ambiguities arise, and semantic analysis, however primitive, must be performed. It was decided to leave these two problems for later stages of the project. Syntactic analysis, when implemented, would rely on information from the dictionary, and semantic analysis will be limited to checking up collocations in the dictionary – that is, deciding in favour of words that typically occur in particular contexts related to other words, rather than in favour of words that do not. The information on collocations in Serbian language will be acquired through statistical analysis of very large textual databases, and entered into the dictionary along with other information.

Another problem that occurs is that some words may not be found in the dictionary. It can happen because of their rarity, because a nonstandard affix was used, but also frequently in case of foreign names, names of companies etc. In that case, strategies for determining the correct way of stressing must be defined. Strategies currently being developed within our projects include making analogies based on standard prefixes and suffixes and rhyming.

The graphical user-interface created for entering words in the dictionary is dialog-based and highly intuitive. The person entering the dictionary must be familiar with lexis of

stress system in Serbian, and must be able to stress words properly. However, after a short introduction, even a lay user of the TTS system is able to add words to the dictionary if desired. For instance, he/she might want to enter names of employees in his/her call centre.

#### 4.2. $F_0$ codebook

Using information from the dictionary, the system is able to reconstruct a particular stress configuration of a group of words which form a metrical unit. In this phase of the project, several  $f_0$  contours are assigned to each metrical unit, depending on its position in the sentence (beginning, neutral, before comma, ending), and the resulting  $f_0$  contour is smoothed in order to avoid audible pitch discontinuities and tilted towards the end of the sentence [1, 3]. Such a method does not take into account syntactical information, but relies only on punctuation marks. However, results are still significantly better than in case of synthesizers with constant  $f_0$ , available in Serbian until now.

#### 5. ON-LINE SELECTION OF SEGMENTS

Halfphones are considered as basic units which cannot be further segmented, but it is desirable to extract segments as large as possible, in order to preserve intelligibility. According to differences between existing and required values of parameters previously defined, each speech segment which can be extracted and used for synthesis is assigned *target cost*, and according to differences at the boundaries between two segments, each pair of segments which can be concatenated is assigned *concatenation cost* [2]. Target cost is the measure of dissimilarity between existing and required prosodic features of segments, including duration,  $f_0$ , energy and spectral mismatch. Concatenation cost is the measure of mismatch of the same features across unit boundaries. Various phoneme groups are treated in different fashion. Some types of phonemes, such as unvoiced plosives, are more suitable for segmentation than the others, and have lower concatenation costs. The degree of impairment of phones is also taken into account when selecting segments, as explained previously.

The task of the synthesizer is to find a best path through a trellis which represents the sentence, that is, the path along which the least overall cost is accumulated. The chosen path determines which segments are to be used for concatenation, as shown on Figure 2.

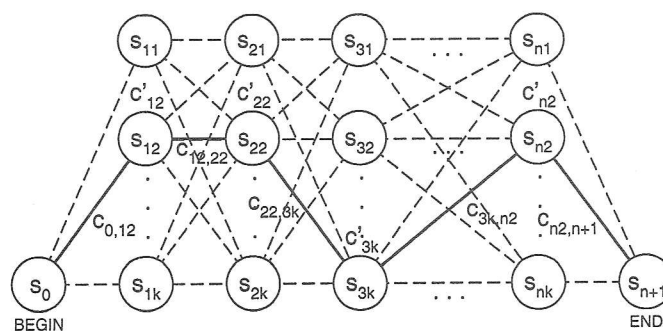


Figure 2. Finding a best path through a trellis representing a sentence

Figure 2. Finding a best path through a trellis representing a sentence

## 6. CONCLUSION

In this paper conception of high-quality TTS in Serbian language is described in detail. Prosody generation principles are presented, in view of several distinctive features of Serbian language. On-line selection of speech segments to be concatenated according to predefined criteria aimed at minimizing audible discontinuities leads to fairly intelligible and natural-sounding synthetic speech. After several previous attempts at creating a TTS system in Serbian which were mostly diphone-based and did not treat prosody in any way, this is the first complete TTS in Serbian which is commercially applicable.

## 7. REFERENCES:

- [1] T. Dutoit: *An Introduction to Text-to-Speech Synthesis*, Kluwer Academic Publishers, Dordrecht/ Boston/London, 1997.
- [2] M. Beutnagel, M. Mohri, M. Riley: Rapid Unit Selection from a Large Speech Corpus for Concatenative Speech Synthesis, *Proceedings of EUROSPEECH '99*, pp.607-610. Budapest, Hungary, 1999.
- [3] I. Lehiste, P. Ivić: Word and Sentence Prosody in Serbocroatian, The Massachusetts Institute of Technology, 1986.
- [4] V. Delić, S. Krčo, D. Glavatović: Basic Elements for ASR and TTS in Serbian Language, *DOGS*, pp. 32-37, Fruška Gora, maj 1998.
- [5] M. Sečujski: Text-to-Speech with Respect to Serbian Language, graduation thesis, School of Engineering, Novi Sad, 1999.
- [6] M. Sečujski: Stress Dictionary of Serbian Language Intended for TTS, *DOGS*, Bečej, 2002.
- [7] D. Pekar, R. Obradović: AlfaNum System for Continuous Speech Recognition, *TSD 2002*, Brno, Czech Republic, 2002.
- [8] R. Obradović, D. Pekar: C++ Library for Signal Processing – SLIB, *DOGS*, Novi Sad, 2000.

## INFLUENCE OF LOADED WAGON ON ELECTROMAGNETIC FIELD DISTRIBUTION IN MINE PIT

*Dijana G. Borisov, Sasa S. Ilic, Faculty of Electronic Engineering in Nis, Beogradska 14, 18000 Nis, Yugoslavia*

**Abstract:** *Electromagnetic field distribution in a mine pit is approximately numerically determined, when the slit coaxial lines are used for realizing a radio link and the progressive TEM wave propagates on them. Calculations are based on the equivalent electrodes method. Numerical results for equipotential and equienergetic surfaces of slit coaxial line in the mine pit, when loaded wagon is in are presented in this paper. Influence of wagon and shape of loading on the field distribution is investigated. Influence of slit coaxial line position and angular opening position of slit coaxial line on the field distribution is also investigated.*

**Keywords:** *Electromagnetic field, Slit coaxial line, Radio link, Mine pit*

### 1. INTRODUCTION

Directional antennas set at the ends of the tunnel, or slit coaxial lines drawn through the tunnel are used for realizing a radio link space-time continuum between a locomotive and a dispatcher center, in the case of a train is in the tunnel, in the enclosed steel bridge or in the mine pit.

Consequently, slit coaxial lines as well as electromagnetic field which slit coaxial lines produce in the tunnels and bridges have been an object of several investigations [1-7]. The equivalent electrodes method, which has been developed at the Faculty of Electronic Engineering in Nis, proved as a very useful method for solving the lines with slit shields [8].

This method is also applied for determining the electromagnetic field that slit coaxial lines produce in mine pits, in the case when loaded wagon is inside. For this purpose, it is adopted that the progressive TEM waves propagate on the slit coaxial line alone, assuming the mine walls, wagon, load and earth surface are perfectly conductive. The calculations are based on the equivalent electrodes method, considering the influence of the wagon and mine pit on the slit line and conversely. A developed program package TUNNEL [9] provides a variety of possibilities for users. Above all it is the possibility of a true setting of the size and shape of the wagon and load, and the shape of the mine pit walls.

As a result of the calculation the values for characteristic impedance and resistance per unit line length of the coax with axial slit are obtained. The values for potential and electric and magnetic field strengths in a prescribed region of interest are also obtained. Map of equi-potential surfaces, as well as of equienergetic surfaces, defining a geometric position of the points of constant intensity of the electric and magnetic field strength, or of constant densities of the energies located in the field, can also be obtained.

### 2. MATHEMATICAL MODEL OF MINE PIT

The aim of this paper is to determine the electromagnetic field distribution in a mine pit, when the loaded wagon is inside. For this purpose, a mathematical

model of the mine pit with built-in coaxial line with axial slit has been derived (Figs.1 and 2). The shape of load is approximated by means of flat and oval parts (Fig.1), and of oval parts (Fig.2).

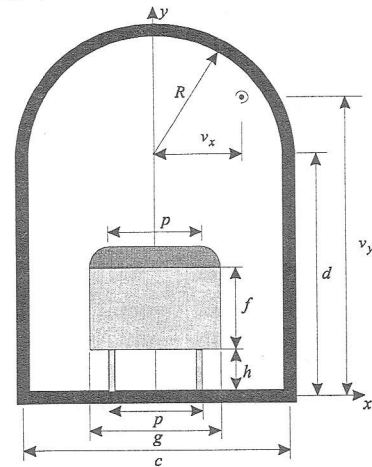


*Fig. 1: Mathematical model of mine pit, when loaded wagon is inside and shape of load is approximated by means of flat and oval parts*

There, the mine pit cross section is considered to be rectangular and the roof is approximated by means of half-circle. The mine pit walls, as well as the earth surface are assumed to be perfectly conductive. It is adopted that the wagon cross section is rectangular, considering wheels and gaps existing under the wagon.

User sets the positions of coaxial line with axial slit and its angular opening. The slit coaxial line position is determined by its axis co-ordinates,  $v_x$  and  $v_y$  (Figs.1 and 2).

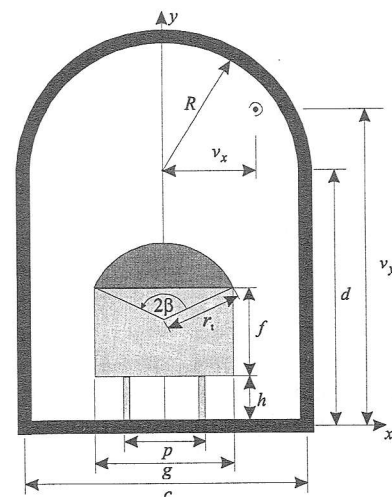


*Fig. 2: Mathematical model of mine pit, when loaded wagon is inside and shape of load is approximated by means of oval parts*

The shield slit position is determined by the angle  $\theta_x$  (Fig.3). Radius of the interior conductor of slit coaxial line is denoted as  $a$ , of shield as  $b$  and angular width of the shield slit as  $2\alpha$ .

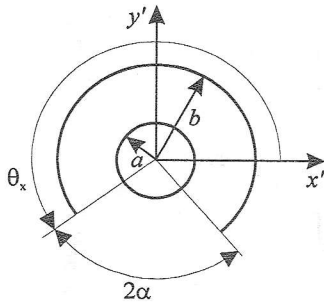


Fig. 3: Shield slit position

### 3. NUMERICAL RESULTS

Calculations of electromagnetic field distribution and potential are done by use of the equivalent electrodes method. Because this method and its application are detailed presented in [8-12], therefore only the obtained results will be presented in this paper.

It is considered the mine pit having dimension given in Table 1.

It is investigated two different positions of slit coaxial line: position 1 -  $v_x/a = 0$  and  $v_y/a = 3850$ , and position 2 -  $v_x/a = 1350$  and  $v_y/a = 2500$ .

Table 1. (Figs.1 and 2)

$b/a = e$	$R/a = 1500$	$p/a = 800$
$\alpha = 50^\circ$	$c/a = 3000$	$f/a = 1000$
$d/a = 2500$	$g/a = 1200$	$h/a = 400$
$\beta = 53.13^\circ$	$Rt/a = 750$	

For each position of slit coaxial line, it is investigated the cases when the shield slit is orientated to the wagon, case A -  $\theta_x = 220^\circ$ , and to the wall of mine pit, case B -  $\theta_x = 40^\circ$ .

Equipotential and equienergetic surfaces of the coaxial line with axial slit in the mine pit, when the loaded wagon is in the mine pit and when the coaxial line is in position 1, and in position 2 are shown in Figs. 4-7.

Loaded wagon has a great influence on electromagnetic field distribution in the mine pit (Tables 2 and 3). Shape of load also influences on electromagnetic field distribution in the mine pit. For position 1 of coaxial line, shield slit position does not influence on electromagnetic field distribution. For position 2 of coaxial line, shield slit position appreciably influences on electromagnetic field distribution.

### 4. CONCLUSION

The electromagnetic field distribution in a mine pit is determined by means of the equivalent electrodes method, when the slit coaxial lines are used for realizing a radio link and a progressive TEM wave is excited on them. The influence of loaded wagon and shape of load on the electromagnetic field distribution is investigated. The influence of slit co-axial line position and angular opening position of slit coaxial line on the electromagnetic field distribution is also investigated.

### 5. REFERENCES

- [1] Duncan, J. W., Minerva, V. P.: *Bandwitch Balun Transformer*, Proc. IRE, vol.48, pp. 156-164, Feb. 1960.
- [2] Gunston, M. A. R.: *Microwave Transmission - Line Impedance Data*, Van Nostrand Reinhold Company LTD, New York, Cincinnati, Toronto, Melbourne, 1972.
- [3] Velickovic, D. M.: *Slit Cable Calculation*, EUROEM, pp. THp-04-06, Bordeaux, 30 May-June 4, 1994.
- [4] Velickovic, D. M.: *Calculation of Characteristic Impedance of Coax with Axial Slit*, RAILWAYS, No. 11-12, pp. 669-671, 1996.
- [5] Velickovic, D. M.: *TEM Analysis of Transmission Lines Using Equivalent Electrodes Method*, TELSIKS97, Nis, Vol. I, pp. 64-74, 8-10 October 1997.
- [6] Velickovic, D. M., Mancic, Z. J., Zulkic, D. G.: *Retangular Coax with Axial Slit and with Rectangular or Circular Center Conductor*, EMC'98 ROMA, pp. 384-389, Rome, Italy, 14-18 September 1998.
- [7] Velickovic, D. M., Mancic, Z. J., Zulkic, D. G.: *Axial Slit on Two Wire Line with Rectangular Shield*, ANALELE UNIVERSITATII DIN ORADEA, Fascicola ELECTROTEHNICA, pp. 18-23, Felix-Spa, Romania, 27-30 May 1998.
- [8] Velickovic, D. M.: *Equivalent Electrodes Method*, SCIENTIFIC REVIEW, pp. 207-248, Belgrade, 1996.
- [9] Velickovic, D. M., Ilic, S. S., Zulkic, D. G.: *Computer Program TUNNEL*, Technical Report, Department of Theoretical Electrotechnics, Faculty of Electronic Eng., University of Nis, 1998.
- [10] Velickovic, D. M., Ilic, S. S., Zulkic, D. G.: *Electromagnetic Field of Coaxial Lines with Axial Slit in a Tunnel or on an Enclosed Bridge - Theoretical Analysis*, ICATE 2000, pp. 7-10, Craiova, Romania, May 25-28, 2000.
- [11] Ilic, S. S., Zulkic, D. G.: *Electromagnetic Field of Coaxial Lines with Axial Slit in a Tunnel or on an Enclosed Bridge - Theoretical Analysis*, ETRAN 2000, pp. 195-198, Sokobanja, 26-29 June 2000.
- [12] Zulkic, D. G., Ilic, S. S.: *Electromagnetic Field of Coaxial Lines with Axial Slit in Mine Pits*, ETRAN 2001, pp. 198-201, Bukovicka Banja, 4-7 June 2001.

## 6. APPENDIX

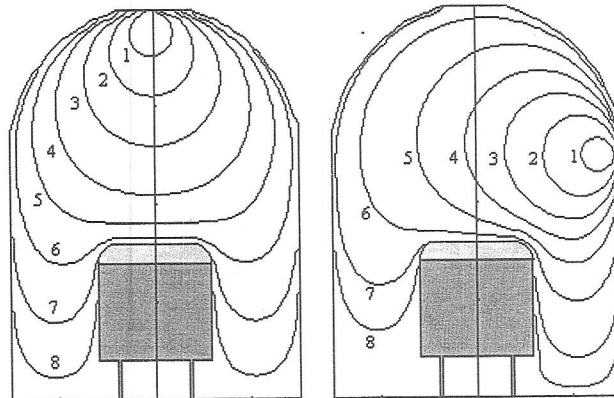


Fig. 4: Equipotential surfaces of coaxial line with axial slit in the mine pit when loaded wagon is inside, when load is approximated by means of flat and oval parts, and when coaxial line is in position 1, and position 2

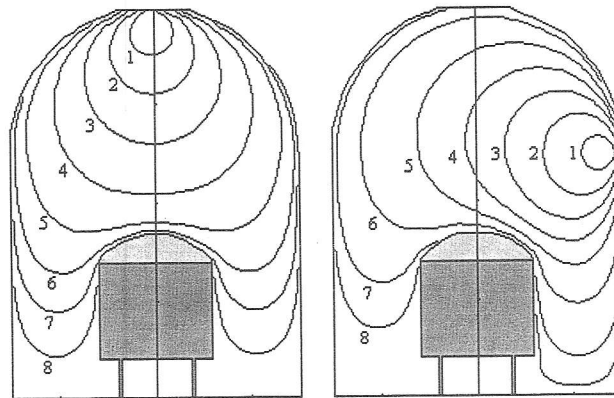


Fig. 5: Equipotential surfaces of coaxial line with axial slit in the mine pit when loaded wagon is inside, when load is approximated by means of oval parts, and when coaxial line is in position 1, and position 2

Table 2.  $10^3 \varphi/U$

No.	Fig.1, position 1		Fig.1, position 2		Fig.2, position 1		Fig.2, position 2	
	Case A	Case B						
1	8.62405	8.62405	11.7819	11.6908	8.61970	8.61970	11.7783	11.6869
2	3.89628	3.89628	4.76278	4.70965	3.88656	3.88656	4.74838	4.69507
3	1.82016	1.82016	2.44365	2.41901	1.79911	1.79911	2.41126	2.38727
4	0.76901	0.76901	1.31867	1.30883	0.71901	0.71901	1.27910	1.27043
5	0.29602	0.29602	0.59908	0.59621	0.20052	0.19529	0.57386	0.57180
6	0.06363	0.06210	0.15293	0.15237	0.04664	0.04549	0.14623	0.14589
7	0.00775	0.00756	0.01920	0.01676	0.01145	0.01116	0.02001	0.01748
8	0.00091	0.00091	0.00368	0.00321	0.00220	0.00220	0.00383	0.00335

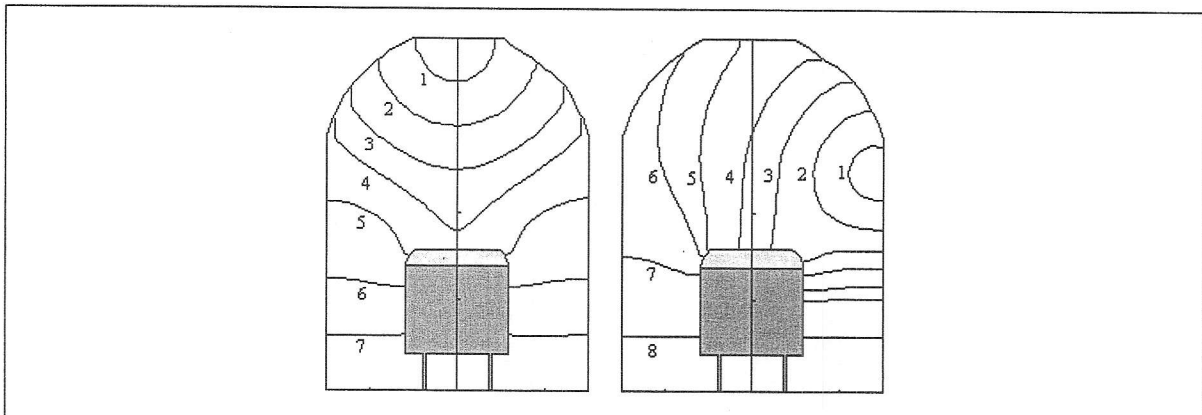


Fig. 6: Equipotential surfaces of coaxial line with axial slit in the mine pit when loaded wagon is inside, when load is approximated by means of flat and oval parts, and when coaxial line is in position 1, and position 2

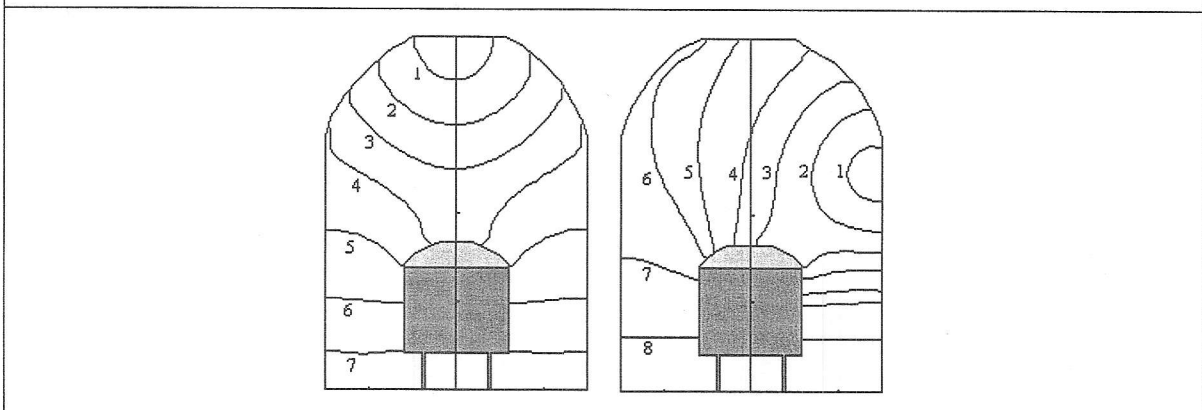


Fig. 7: Equipotential surfaces of coaxial line with axial slit in the mine pit when loaded wagon is inside, when load is approximated by means of oval parts, and when coaxial line is in position 1, and position 2

Table 3.  $10^6 a|E|/U$

No	Fig.1, position 1		Fig.1, position 2		Fig.2, position 1		Fig.2, position 2	
	Case A	Case B						
1	22.0796	22.0796	37.0970	36.7579	22.0908	22.0908	37.1140	36.7735
2	5.20745	5.20745	8.68048	8.58077	5.22558	5.22558	8.71993	8.61915
3	2.40745	2.40745	3.85072	3.81158	2.44604	2.44604	3.89358	3.85454
4	1.50464	1.50464	2.03306	2.01785	1.31077	1.26442	2.03375	2.01993
5	0.79601	0.77423	1.02164	1.01674	0.45953	0.44783	0.98963	0.98607
6	0.11210	0.10941	0.64002	0.63254	0.05787	0.05644	0.59114	0.58527
7	0.01382	0.01349	0.14751	0.14564	0.00737	0.00719	0.14224	0.14069
8			0.00945	0.00933			0.00935	0.00925

## ANALYSIS OF NEURAL NETWORK MODELS OF SERBIAN SPEECH CONSONANTS

Danijela Arsenijevic, Institute of Applied Mathematics and Electronics, Kneza Milosa 37, Belgrade  
Milan Milosavljevic, Faculty of Electrical Engineering Belgrade, Bulevar Kralja Aleksandra 73

**Abstract:** In this paper, neural autoregressive model (NNAR) as well as linear autoregressive model (AR) of consonants and sonants of Serbian language, was evaluated, and final prediction gain of models was proposed.

**Keywords:** speech, AR model, NNAR model, sonants, and consonants.

## 1. INTRODUCTION

Human speech system is highly nonlinear structure. When it should be modeled few characteristics have to be considered: vocal tract, oral tract and nasal tract transfer functions as well as excitation type. Pharynx, the velum and the articulators, including the teeth, tongue, palate, lips and the jaw, play significant role in speech production [7]. We examined two models: linear autoregressive model (AR) [2] and nonlinear model (NNAR) determined as transfer characteristic of feedforward neural network. Experiments were made on unwoveled speech in serbian language, for both sexes speakers. Earlier in papers we showed that 10-th order AR model as well as corresponding NNAR model gave good results in wovel speech signal prdiction (a, e, i, o, u) [5, 6, 7, 8]. That can be explained with quasiperiodical exitation and closed nasal tract at the moment when those sounds have to be formed. For a very long period of time vowels are quasiperiodical and also sonorous, witch is very convenient when diferent models have to be evaluate. Unwoveled signals last briefly and could be sonorous or voiceless, could be sonants or consonants, and they can take rise at lips, teeth, alveolas, plates and so on [1]. Those characteristics made unwoveled phonemes extremely inconvenient when we have to model speech system, so the purpose of this paper was the evaluation of standard linear and nonlinear models efficiency calculated on isolately spoken sonants and consonants of serbian language. Second part of this paper is about theoretical base of experiments, third part is about experimental results and fourth part is conclusion.

## 2. MODELS

We used linear  $p$ -th degree AR model given by:

$$y(n) = \sum_{i=1}^p a_i y(n-i) + e(n), \quad (1)$$

where  $y(n)$  is sample of speech signal,  $e(n)$  is error and  $a_i$  is model parameter. As nonlinear model example NNAR model is given with:

$$g(y(t), \delta(t), t) = \varepsilon(t), \quad (2)$$

where  $\delta^T(t) = [-y(t-1), \dots, y(t-n)]$  is  $n$  samples vector,  $\varepsilon(t)$  is error and  $g$  is nonlinear parametric transfer function known in advance. Function  $g$  is modelled by feedforward neural network with one hidden layer as in Fig.1. Output of this structure is determined as in (3):

$$y_i(\mathbf{w}, \mathbf{W}) = F_i \left( \sum_{j=1}^q W_{ij} f_j \left( \sum_{l=1}^m w_{lj} z_l + w_{j0} \right) \right) + W_{f0} \quad (3)$$

$y_i$  is output,  $w_i$  and  $W_i$  are weight matrixes and  $f_j$  is  $F_i$ , are transfer functions of hidden and output nodes, respectively,  $q$  is number of hidden nodes and  $m$  is number of elements in input layer [7]. We used Final Prediction Error Gain criteria (in dB) determined as:

$$G_{FPE} = 10 \log \frac{E}{FPE}. \quad (4)$$

Where:

$$E = \frac{1}{N} \sum_{i=1}^N y(i)^2, \quad (5)$$

and

$$FPE = \frac{N+d}{N-d} \left( \frac{1}{N} \sum_{i=1}^N (y(i) - \hat{y}(i))^2 \right), \quad (6)$$

are mean square of training set values and Akaike's Final Prediction Error (FPE), respectively.  $N$  is size of training set and  $d$  is number of free parameters in model [3, 7, 8]. We used standard covariant method for AR model while in neural network case we used Levenberg-Marquart method and Back-Propagation Algorithm for error minimization (BPA) [3,4].

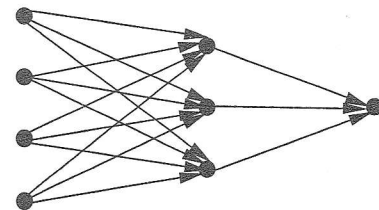


Fig.1 Feedforward neural network

## 3. EXPERIMENTAL RESULTS

Experiments were made on isolately spoken phonemes that both sexes speakers spoke. Analogous signals were digitalized by  $f_s = 22050$  Hz (PCM, 16b, wav format), and "ə" (closed "e") was rejected. ASCII signals were formed for MATLAB R12 and normalised in  $[-1, 1]$ . 10-th degree AR model and 10-3-1 feedforward neural network were examined. Results are given in Table 1. - Table 4.

Table 1. AR model gain for mail unwoveled phonemes is given, while in Table 2. The same result is given but for femail speaker. In Table 3. NNAR model gain for mail unwoveled phonemes is given, while in Table 4. NNAR model gain for femail unwoveled phonemes is given.

There is grouping that can be catch sight of tables no metter of sexes or model type, for example sonar sonants (j, l, lj, m, n, nj, r) always give larger Gain than other phonemes, sonar consonants (f, c, s, t, č, š, h, k) don't except (b, p). Voiceless sonant "v" gives great amount of gain while voiceless consonants (d, đ, dž, z, ž, g) give medium amount

of FPE gain depending of model or speaker sex. Same results are given graphically for male speaker in Fig.2.. and for female speaker in Fig.3. In Fig.4. the difference for both speakers and both models is given.

Table 1. AR model Gain for male unwoveled phonemes

VOICELESS SONANT								SONAR SONANT				
Gam (dB)	10-15	15-20	20-25	25-30	↑	0-5	5-10	10-15	15-20	20-25	25-30	↑
Usneno-zubni				V								
Alveolarni											R	L, N
Prednjeneb										J	Lj	Nj
Usneni												M
VOICELESS CONSONANT								SONAR CONSONANT				
Gam (dB)	10-15	15-20	20-25	25-30	↑	0-5	5-10	10-15	15-20	20-25	25-30	↑
Usneni								F				B, P
Zubni	Z			D		C, S	T					
Prednjeneb	Dž, Ž, Đ					Č	Č, Š					
Zadnjeneb		G					H	K				

Table 2. AR model Gain for female unwoveled phonemes

VOICELESS SONANT								SONAR SONANT				
Gaz (dB)	10-15	15-20	20-25	25-30	↑	0-5	5-10	10-15	15-20	20-25	25-30	↑
Usneno-zubni			V									
Alveolarni										R	L	N
Prednjeneb											J	Lj, Nj
Usneni												M
VOICELESS CONSONANT								SONAR CONSONANT				
Gaz (dB)	10-15	15-20	20-25	25-30	↑	0-5	5-10	10-15	15-20	20-25	25-30	↑
Usneni						F						B
Zubni	Z				D	C, S	T					
Prednjeneb		Dž, Ž	Đ				Č	Č, Š				
Zadnjeneb				G				H	K			

Table 3. NNAR model Gain for male unwoveled phonemes

VOICELESS SONANT								SONAR SONANT				
Gnm (dB)	10-15	15-20	20-25	25-30	↑	0-5	5-10	10-15	15-20	20-25	25-30	↑
Usneno-zub				V								
Alveolarni												RLN
Prednjenebč										J		Lj, Nj
Usneni												M
VOICELESS CONSONANT								SONAR CONSONANT				
Gnm (dB)	10-15	15-20	20-25	25-30	↑	0-5	5-10	10-15	15-20	20-25	25-30	↑
Usneni								F				B, P
Zubni	Z				D		C, S	T				
Prednjeneb		Dž, Ž, Đ						Č, Č	Š			
Zadnjeneb			G					H	K			

Table 4. NNAR model Gain for female unwoveled phonemes

VOICELESS SONANT								SONAR SONANT				
Gnz (dB)	10-15	15-20	20-25	25-30	↑	0-5	5-10	10-15	15-20	20-25	25-30	30 ↑
Usneno-zubni			V									
Alveolarni											R	L, N
Prednjene												J, Lj, Nj
Usneni												M
VOICELESS CONSONANT								SONAR CONSONANT				
Gnz (dB)	10-15	15-20	20-25	25-30	↑	0-5	5-10	10-15	15-20	20-25	25-30	30 ↑
Usneni					D	F		P				B
Zubni	Z					C, S		T				
Prednjene		Dž, Ž			Đ			Č, Š	Č			
Zadnjeneb					G			H		K		

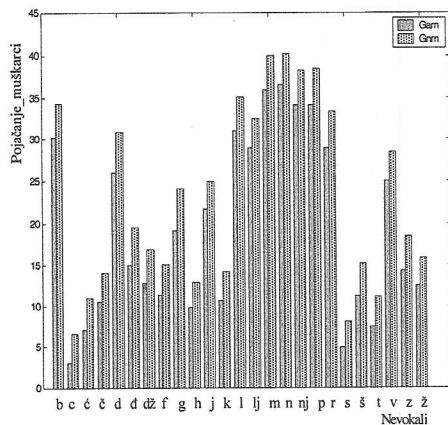


Fig.2. FPE Gain-male speaker

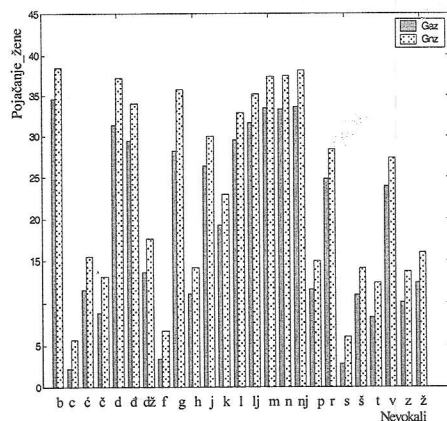


Fig.3. FPE Gain-female speaker

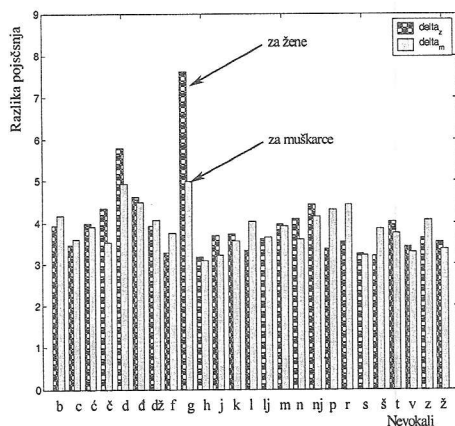


Fig.4. FPE Gain difference-both speakers

#### 4. CONCLUSION

This paper presents results of experimental analysis on Serbian male and female phonemes. Closed "e", "d", was rejected to every phoneme. Analogous phonemes were sampled with  $f_s=22050\text{Hz}$  (PCM, 16b, wav format) sampling frequency and ASCII signals for MATLAB R12 were formed. AR as well as NNAR models were used to model human speech system. 10-th degree AR model is used to cover frequency domain of 4kHz. 10 inputs, 3 hidden layer neuron with tanh transfer function, and 1 linear output feedforward neural network is used in NNAR modeling. Back-Propagation Algorithm and Levenberg-Marquart

approximation is used for parameter extremization. Evaluated models showed:

- small number of parameters,
  - short training time,
  - easy training algorithms,
- FPE Gain showed:
- FPE Gain for unwoveled phonemes can differ from group to group for a 5dB or more,
  - in the same group FPE Gain can differ for about 5dB. That is determined with origin of phonemes, sonority and so on
  - FPE Gain of AR models for female speakers can be to 10dB greater than FPE Gain of AR models for male speakers
  - FPE Gain of NNAR models for female speaker can be to 5dB greater than FPE Gain of NNAR models for male speakers
  - There are some grouping no metter of models, sex of speaker and so on. Suppose: sonar sonants (j, l, lj, m, n, nj, r) always give larger Gain than other phonemes, sonar consonants (f, c, s, t, č, š, h, k) don't except (b, p). Voiceless sonant "v" gives great amount of gain while voiceless consonants (d, đ, dž, z, ž, g) give medium amount of FPE Gain depending of model or speaker sex.

#### 5. REFERENCES

- [1] D.G.Childrens, "Speech Processing and Synthesis Toolboxes", John Wiley&Sons, Inc., New York, 2000.
- [2] L.Ljung, "System Identification: Theory for the User", Prentice-Hall, Englewood Cliffs, N.J., 1987.
- [3] M.Norgaard, "Neural Network Based System Identification Toolbox", Version 1.2, Technical University of Denmark, Department of Automation Department of Mathematical Modelling, Technical Report 97-E-851, 2001.
- [4] B.Kovačević, M.Milosavljević, M.Veinović, M.Marković, "Robusna digitalna obrada govornog signala", Akademska misao, Belgrade, 2000.
- [5] M.Obradović, M.Milosavljević, "Digitalna obrada i prepoznavanje signala", Univerzitet Vojske Jugoslavije, Belgrade, 1993.
- [6] Danijela Arsenijević, Milan Milosavljević, "Crosscorelation analysis of internal signals of neural networks trained on Serbian vowels", In J.Đorđević, M.Milosavljević, M.Srećković, P.Pejović, editors, *Proceedings of XLIV conference ETRAN-2000, Sveska III, pages 136-139, Arandjelovac, 2001.*
- [7] Danijela Arsenijević, Milan Milosavljević, "Spectral interpretation of pruned neural network models of speech signal", In R.Petrović and D.Radojević, editors, *Proceedings of the XXVII Yugoslav Conference SYMOPIS, Belgrade, Yugoslavia, 2001.*
- [8] Milan Milosavljević, Danijela Arsenijević, "Analysis of a long term neural network speech model" In R.Petrović and D.Radojević, editors, *Proceedings of the XXVII Yugoslav Conference SYMOPIS, Belgrade, Yugoslavia, 2001.*

## A NOVEL DIRECT TORQUE CONTROL APPROACH IN INDUCTION MACHINE DRIVES

Petar Matić, Branko Blanuša, *Faculty of Electrical Engineering in Banjaluka, Banjaluka, Republic of Srpska*  
Slobodan N. Vukosavić, *Faculty of Electrical Engineering in Belgrade, Belgrade, Yugoslavia*

**Abstract:** – Direct Torque Control (DTC) approach in induction machine drive is important method for de-coupled control of torque and flux. In this paper a novel approach to DTC torque and flux control of induction machine drive is described. This approach is theoretically described, and tested by computer simulation. It is shown that the performances of proposed approach are the same as the performance of more complex solutions.

**Keywords:** Direct Torque Control, Induction Machine Drive

### 1. INTRODUCTION

De-coupled control of induction machine (IM) drive can be achieved by two standard approaches:

- Field Oriented Control (FOC)
- Direct Torque Control (DTC) [1].

FOC of induction machine provides very fast torque and flux control by adjusting the magnetizing and active component of stator current. Magnetizing component drives the flux, and active component drives the torque, reaching performance of IM to be similar as control of DC machine. FOC algorithms demand very fast Current Regulated Pulse Width Modulation (CRPWM) inverter, which builds a cascade consisting CRPWM, PI regulators and coordinate transformations. This cascade degrades the performance of FOC drive in all regimes, particularly in field weakening region, when the inverter voltage is at limit. In field weakening region, available inverter voltage is not sufficient to drive stator currents to achieve accurate control of torque and flux. In addition, FOC is very complex concept and parameter sensitive. [1,2].

DTC control of induction machine drive provides a very quick and precise torque response without the complex field – orientation block and the inner current regulation loop. This makes possible to achieve better control of torque and flux than FOC in all regimes, particularly in field weakening region. DTC approaches are newer than FOC, having rapid growth in recent years. There is no standard for DTC classification yet, but most interesting approaches can be classified as in [1-7].

### 2. RECENT DTC APPROACHES IN INDUCTION MACHINE DRIVE

In the literature there are two main DTC approaches [1-7]. Both of them tend to generate such stator voltage, which will drive torque and flux errors down to zero. This results torque and flux to reach commanded references as fast as possible with minimal error during the period  $\Delta T$ . Torque and flux errors during the period  $\Delta T$  are defined as:

$$\Delta m = m_{k+1} - m_k, \quad (1)$$

$$\Delta \Phi = |\Psi_{k+1}| - |\Psi_k|, \quad (2)$$

where  $m_{k+1}$ ,  $m_k$  are torque reference and estimated torque,  $|\Psi_{k+1}|$ ,  $|\Psi_k|$  are modulus of flux reference and estimated flux, and  $\Delta \Phi$  and  $\Delta m$  are demanded flux and torque increments.

DTC approaches can be classified as [1-7]:

- DTC with discrete stator voltage (DSV) and
- DTC with continuous stator voltage (CSV).

DTC with DSV approaches tend to minimize torque and flux errors (1 and 2) into defined limits for torque and flux errors,  $\Delta H_m$  and  $\Delta H_\psi$ . DTC with CSV approaches drive torque and flux errors (1 and 2) down to zero by using standard Space Vector Width Pulse Modulation (SVPWM) technique to generate desired stator voltage. DSV approaches are very simple and not computer intensive, but as main defect, they have large torque and flux ripple both in steady state and transient regimes. Performances of DTC with CSV approaches in steady state are satisfying, but DTC with CSV has intensive computer calculations necessary to generate desired stator voltage. Besides good performance in steady state, DTC with CSV is very complex approach and in transient regimes has to use DSV concept, what leads to large torque and flux errors in transients. Recent DTC approaches with CSV have to be simplified, and performance in transient regimes, particularly in field weakening regime has to be advanced.

Fig. 1. shows basic DTC approach with DSV block – diagram.

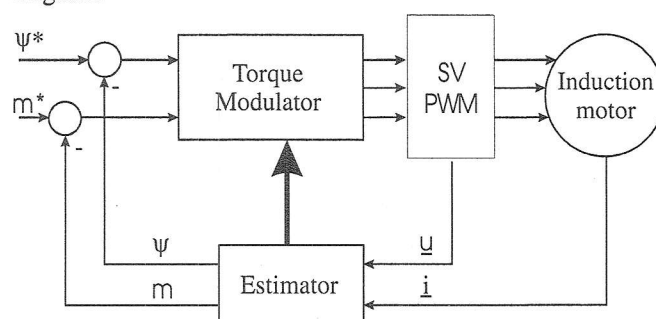


Fig. 1. Basic DTC approach with DSV

Stator voltage reference in stationary reference frame ( $\alpha - \beta$ ) is calculated by solving two equations into block named *Torque Modulator* shown on Fig. 1. Desired flux magnitude and torque increment through the period  $\Delta T$  can be plotted as a line and a circle in  $\alpha - \beta$  plane as functions of necessary stator voltage [1,2,4,5]:

$$\frac{\Delta m_e}{\Delta T} = -m_e \left( \frac{1}{\sigma T_s} + \frac{1}{\sigma T_r} \right) + \frac{3}{2} P \frac{M}{\sigma L_s L_r} [\Psi_{\alpha} u_{\beta} - \Psi_{\beta} u_{\alpha} - \omega_m \Psi_{\alpha} \Psi_{\alpha}] \quad (3)$$

$$\Psi^2(k+1) = (\Psi_\alpha(k) + u_\alpha \Delta T)^2 + (\Psi_\beta(k) + u_\beta \Delta T)^2 \quad (4)$$

Intersect of torque line (3) and flux circle (4) defines desired stator voltage components in  $\alpha - \beta$  reference frame. Those voltages will drive torque and flux errors (1 and 2) down to zero in one sampling period. This principle can be illustrated as on Fig. 2.

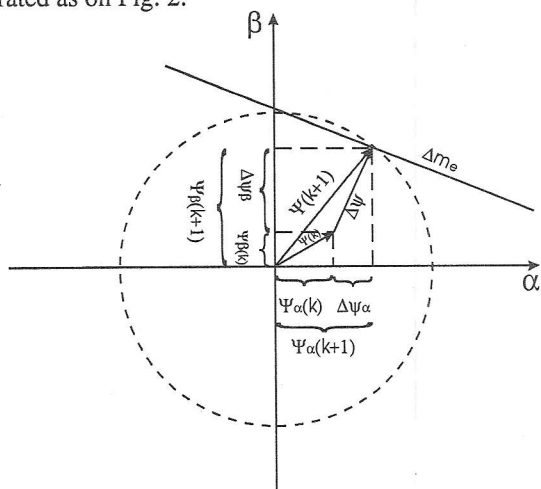


Fig. 2. DTC with CSV in stationary reference frame - standard approach

Desired stator voltage reference,  $\underline{V}_{k+1}$  found from Eq. (3 and 4) is created by SVPWM technique by using two adjacent active vectors and one zero vector.

Basic defect of this concept is finding desired stator voltage vector by solving Eq. 3 and Eq. 4. Those equations can have one, two or no solution for stator reference voltage. When there are two solutions (two working points), there will be two reference voltage vectors that will drive torque and flux errors (1 and 2) down to zero. Selection of optimal working point is made by choosing that stator voltage which will produce smaller stator current [2, 4]. In the other case, when there is no solution of system (3 and 4), there is no intersect of line and circle on Fig. 2, and alternative method has to be selected. This situation appears when torque and flux errors (1 and 2) are too large (particularly in field weakening region), and errors (1 and 2) cannot be driven to zero in just one sample period  $\Delta T$ . In this case, there are two main solutions: restrict reference torque and flux to achieve intersection of line and circle on Fig. 2, or combine CSV technique with DSV technique [5,6,7].

So, main defects of DTC with CSV are:

- Intensive computer calculations - solving the quadratic equation (4) and choosing one optimal of two solutions. This has to be done in every sampling period  $\Delta T$ ;
- Usage of alternative schemes (DTC with CSV) if the solution of Eq. (4) does not exist;
- Usage of trigonometric functions to calculate stator voltage vector components.

Because of complexity, this approach is not applicable in industrial drives, besides good characteristics in steady state. In transient conditions, this approach does not approve good performance.

### 3. A NOVEL DIRECT TORQUE APPROACH

Modification of DTC with CSV, presented in this paper, is based on stator voltage equations in stationary reference frame. Basic idea of this approach is the fact that developed torque is proportional to the stator and rotor flux magnitude, and angle between them, and change in stator voltage vector is proportional to stator flux vector increment:

$$m_e = c \Psi_s \Psi_r \sin \vartheta_{kl}, \quad (5)$$

$$\underline{u}_s = \frac{\Delta \underline{\Psi}_s}{\Delta T}, \quad (6)$$

$$\int \omega_s dt = \int \omega_m dt + \vartheta_{kl}, \quad (7)$$

where:  $\Psi_s$  and  $\Psi_r$  are magnitudes of stator and rotor fluxes,  $\vartheta_{kl}$  is the slip angle,  $\underline{u}_s$  and  $\Delta \underline{\Psi}_s$  are stator voltage and stator flux increment vectors, and  $\omega_s$  and  $\omega_m$  are stator flux frequency and mechanical speed.

In stationary reference frame ( $\alpha - \beta$ ) stator flux vector from previous instant,  $\underline{\Psi}_k$ , and desired flux vector in next instant,  $\underline{\Psi}_{k+1}$ , can be plotted as shown on Fig. 3. In general case, when  $|\underline{\Psi}_{k+1}| \neq |\underline{\Psi}_k|$ , stator flux vector tip  $\underline{\Psi}_{k+1}$  is located on circle  $K_2$ , whose diameter can be larger or smaller than the diameter of circle  $K_1$ . If the stator flux increment module  $\Delta \Phi$  is equal to zero ( $|\underline{\Psi}_k| = |\underline{\Psi}_{k+1}|$ ), then desired stator flux vector tip  $\underline{\Psi}_{k+1}$  is located on circle  $K_1$ . Increasing the stator flux magnitude is proportional to stator flux diameter to increase, and vice versa.

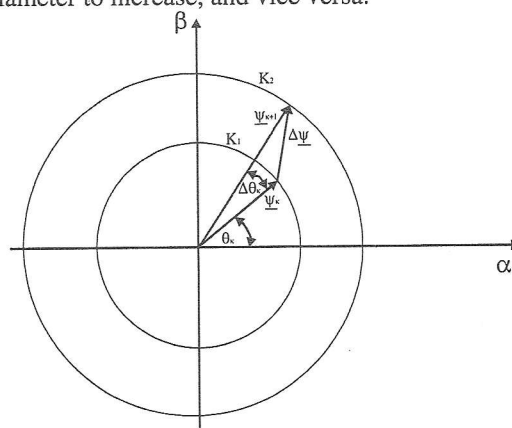


Fig. 3. Definition of stator flux increment vector  $\Delta \underline{\Psi}$

Change in torque,  $\Delta m$ , is the function of previous and next stator flux vector,  $\underline{\Psi}_k$  и  $\underline{\Psi}_{k+1}$ , more exactly their magnitudes  $|\underline{\Psi}_k|$  и  $|\underline{\Psi}_{k+1}|$  and the angle  $\Delta \vartheta$  between them. Increasing the angle  $\Delta \vartheta$  by the same  $|\underline{\Psi}_k|$  и  $|\underline{\Psi}_{k+1}|$  will produce machine torque to increase and vice versa. Fig. 3. shows recent and desired flux vectors, and angle  $\Delta \vartheta$  which produces desired changes in torque.

A new DTC approach will be now explained in detail. Stator flux vector  $\underline{\Psi}_k$  from previous instant is known, in other words diameter of circle  $K_1$  and the stator flux angle  $\vartheta_k$  are known. Reference flux magnitude  $|\underline{\Psi}_{k+1}|$  and torque error  $\Delta m$  are given. It is necessary to calculate the unique

stator flux increment  $\Delta\Psi$  which will drive torque and flux errors,  $\Delta m$  and  $\Delta\Phi$ , down to zero. In this approach, DTC is achieved by calculating stator flux vector  $\Delta\Psi$  (Fig. 3) that will meet the condition:

$$\Psi_{k+1} = \Psi_k + \Delta\Psi. \quad (8)$$

The algorithm of proposed approach is shown on Fig. 4. Knowing torque and flux errors  $\Delta m_e$  and  $\Delta\Phi$ , and machine state vector  $\underline{x}(\omega_s, \omega_{kl}, \Psi_k, |\Psi_{k+1}|)$  desired angle  $\Delta\vartheta = f(\Delta m_e, \Delta\Phi, \underline{x})$  is calculated first. The angle  $\Delta\vartheta$  determines the position of new stator flux vector  $\Psi_{k+1}$  toward to the flux from the previous instant  $\Psi_k$ . Then the desired stator flux vector increment  $\Delta\Psi$  can be calculated, and the unique solution for stator voltage vector is found.

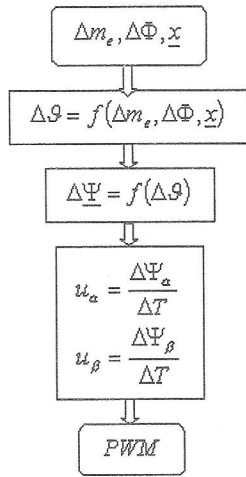


Fig. 4. Algorithm of new DTC approach

Equation for torque production can be linearised through the sampling period  $\Delta T$  as:

$$\Delta m_e = \frac{3}{2}P(\Psi_s \times \Delta i_s) + \frac{3}{2}P(\Delta\Psi_s \times i_s). \quad (9)$$

From Eq. (9) stator current and derivative of stator current can be eliminated by using IM stator voltage equations and equivalent circuit of inverter – driven induction machine shown on Fig. 5.  $L_{\gamma s} = \sigma L_s$  is the transient inductance, and  $\sigma = 1 - M^2 / L_s \cdot L_r$  is the leakage coefficient.

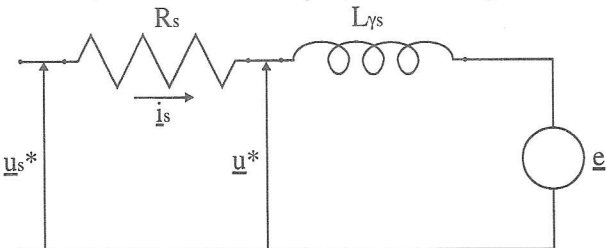


Fig. 5. Equivalent circuit of inverter – driven induction machine

Change in stator current (assuming  $\Delta T \ll L_s / R_s$ ) is:

$$\Delta i_s = \frac{u^* - e}{\sigma L_s} \Delta T, \quad (10)$$

and back EMF, assumed to be sinusoidal with synchronous frequency is:

$$e = j\omega_s(\Psi_s - \sigma L_s i_s), \quad (11)$$

Rotor circuit dynamic has to be considered. In that purpose, rotor voltage equations together with flux equations have to be used [2]:

$$0 = R_r i_r + \frac{\Delta\Psi_r}{\Delta T} - j\omega_m \Psi_r, \quad (12)$$

$$\Psi_s = L_s i_s + M i_r, \quad \Psi_r = L_r i_r + M i_s. \quad (13)$$

Total differential of (13) is:

$$\Delta\Psi_r = \frac{L_r}{M}(\Delta\Psi_s - \sigma L_s \Delta i_s), \quad (14)$$

and Eq. (12 – 14) are substituted in (10), what gives:

$$i_s = \frac{(1 + (\omega_e - \omega_m)^2 \sigma T_r^2) + j(\omega_e - \omega_m) T_r (1 - \sigma)}{L_s (1 + (\omega_e - \omega_m)^2 \sigma^2 T_r^2)} \Psi_s \quad (15)$$

Desired change in torque, represented through the angle  $\Delta\vartheta$  and assuming  $\cos \Delta\vartheta = 1$ ,  $\sin \Delta\vartheta = \Delta\vartheta$  is:

$$\Delta\vartheta = \frac{2\sigma L_s [1 + \omega_{kl}^2 \sigma^2 T_r^2]}{3P(1 - \sigma) |\Psi_k| |\Psi_{k+1}|} \Delta m_e + \frac{|\Psi_k|}{|\Psi_{k+1}|} \omega_e \Delta T - \frac{\Delta\Phi \omega_{kl} \sigma T_r}{|\Psi_{k+1}|} \quad (16)$$

When there is no change in torque ( $\Delta m_e = 0$ ) and no change in stator flux magnitude ( $|\Psi_k| = |\Psi_{k+1}|$ ), stator flux vector increment angle is  $\Delta\vartheta = \omega_s \Delta T$ , what means that the stator flux continues to rotate by synchronous speed. If there is no change in flux ( $\Delta\Phi = 0$ ), and the torque has to be increased, it can be seen from Eq. (16) that the stator flux vector increment angle has to be increased (and vice versa). If there is a change both in stator flux magnitude and torque, stator flux vector increment angle can be increased or decreased depending on torque and flux errors (1 and 2).

From Fig. 3, and assuming  $\cos \Delta\vartheta \approx 1$ ,  $\sin \Delta\vartheta \approx \Delta\vartheta$ , stator flux vector components are:

$$\Delta\Psi_\alpha = \Delta\Phi \cos \vartheta_k - |\Psi_{k+1}| \sin \vartheta_k \cdot (\Delta\vartheta_k), \quad (17)$$

$$\Delta\Psi_\beta = \Delta\Phi \sin \vartheta_k + |\Psi_{k+1}| \cos \vartheta_k \cdot (\Delta\vartheta_k). \quad (18)$$

Cosine and sine functions of angle  $\vartheta_k$  in Eq. (17 and 18) do not have to be calculated, because they can be determined by projections of  $\Psi_k$  as:

$$\cos \vartheta_k = \Psi_{\alpha k} / \sqrt{\Psi_{\alpha k}^2 + \Psi_{\beta k}^2}, \quad (19)$$

$$\sin \vartheta_k = \Psi_{\beta k} / \sqrt{\Psi_{\alpha k}^2 + \Psi_{\beta k}^2}. \quad (20)$$

Stator voltage vector reference can be calculated as:

$$u_\alpha = R_s i_\alpha + \frac{\Delta\Psi_\alpha}{\Delta T}, \quad (21)$$

$$u_\beta = R_s i_\beta + \frac{\Delta\Psi_\beta}{\Delta T}. \quad (22)$$

In field weakening region, stator IR drop in Eq. (21) and (22) can be neglected.

#### 4. SIMULATION OF PROPOSED DTC APPROACH

Proposed DTC approach is illustrated by computer simulation. Fig. 6-8 show characteristic diagrams. Motor parameters are:  $P_n=0,75\text{kW}$ ;  $n_n=1410\text{ rpm}$ ;  $\cos\varphi_n=0,71$ ;  $f_n=50\text{ Hz}$ ,  $L_{\gamma s}=22\text{mH}$ ,  $R_s=10,4\Omega$ ,  $R_r=11,6\Omega$ ,  $L_{\gamma r}=22\text{mH}$ ,  $M=0,557\text{H}$ ,  $J_m=0,0025\text{kgm}^2$ .

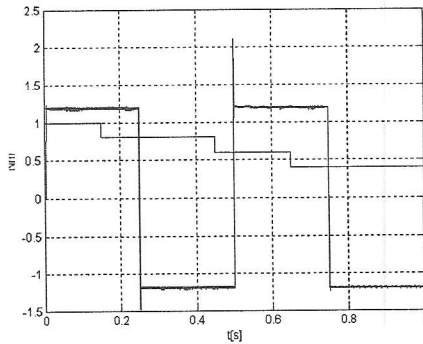


Fig. 6. Reference torque, motor torque, and load torque

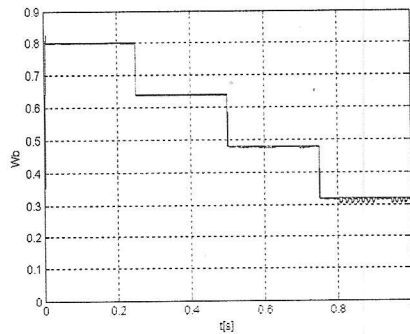


Fig. 7. Reference and estimated stator flux magnitude

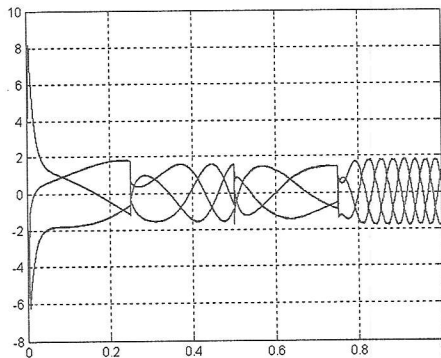


Fig. 8. Stator currents

## 5. CONCLUSION

In this paper a new DTC approach is presented. This approach is based on calculating the desired stator flux angle increment, and stator flux vector increment. This approach gives the unique solution for stator voltage reference, and it has no trigonometric functions, so it is much simpler than other DTC CSV methods. Torque and flux responses are the same or even better than other much-complicated approaches. Characteristics of a novel DTC approach proposed in this paper are theoretically analyzed and illustrated by computer simulation.

## 6. REFERENCES

- [1] Peter Vas: *Sensorless Vector and Direct Torque Control*, Oxford University Press, London, 1998.
- [2] Barbara H. Kenny *Direct Torque Control of Induction Machine Using Self-Sensing at Low and Zero Speed*, Ph. D. Thesis, University of Wisconsin - Madison, 2000.
- [3] Takahashi Isao, Noguchi Toshihiko: "A New Quick-Response and High-Efficiency Control Strategy of an Induction Motor" *IEEE Transactions on Industry Applications*, Vol. IA-22, No.5, Sept/Oct 1986.
- [4] Cristian Lascy, Ion Boldea, Frede Blaabjerg: "A Modified Direct Torque Control for Induction Motor Sensorless Drive", *IEEE Transactions on I. A.*, Vol. 36, No. 1, Jan 2000.
- [5] Thomas G. Habetler, Francesco Profumo, Michele Pastorelli, Leon M. Tolbert: "Direct Torque Control of Induction Machines Using Space Vector Modulation", *IEEE Trans. on Industry Applications*, vol 28, No.5, Sept/Oct 1992.
- [6] Giovanni Griva, Thomas G. Habetler: "Performance Evaluation of a Direct Torque Controlled Drive in the Continuous PWM-Square Wave Transition Region", *IEEE Transactions on Power Electronics*, Vol. 10, No.4, July 1995.
- [7] Barbara H. Kenny, Robert D. Lorenz: "Stator and Rotor Flux Based Deadbeat Direct Torque Control of Induction Machines", *IEEE Transactions on Industrial electronics*, Vol 30, No. 4 2001.

## A POSSIBILITY OF DIGITAL IMAGE COMPRESSION BASED ON CONDITIONAL PROBABILITIES

*Djordje Djurdjevic, Dragi Dujkovic, Milka Potrebic, Faculty of Electrical Engineering Belgrade*

**Abstract:** This paper presents a method of compression of a gray-scale digital image with loss. The method is based on prediction according to conditional probabilities established on the image that is to be compressed.

**Keywords:** Gray-scale digital image compression, conditional probabilities.

### 1. INTRODUCTION

A gray-scale digital image consists of a rectangular matrix which elements represent the illumination intensities. Having in mind the limits of human visual perception, but also some practical reasons, 256 levels of intensity are considered to be satisfactory. Illumination intensity of value 0 represents the black colour, while the intensity of value 255 represents the white colour. The practical reason, mentioned above, is the fact that the memory unit – byte – has the possibility to store 256 different values, which can be interpreted as intensity levels.

### 2. TECHNICAL DETAILS

#### 2.1. A digital image as a set of superimposed bit-planes

As it was already mentioned, every pixel is represented by a single byte and can store a value in the range from 0 to 255. It is possible to extract a specific bit (or bits) in each pixel and use them for display [1]. As an example, Figure 1a shows the original image, while Figures 1b, 1c, 1d, 1e, 1f, 1g, 1h and 1i show separately the single bit-planes. On Figure 1j is shown the original image with the topmost three bit-planes turned on.

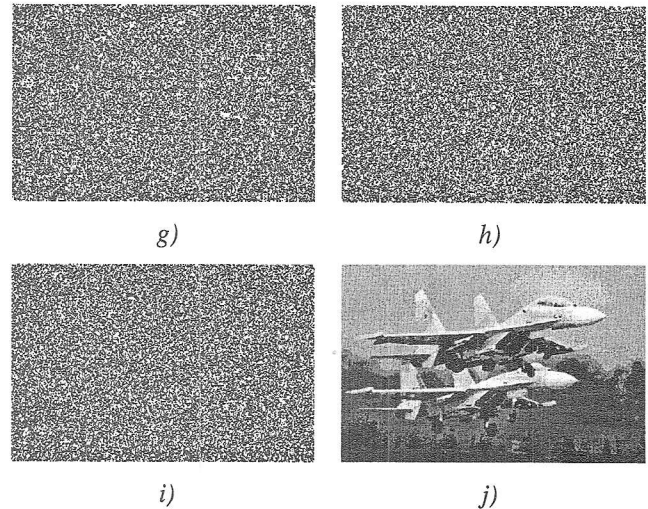
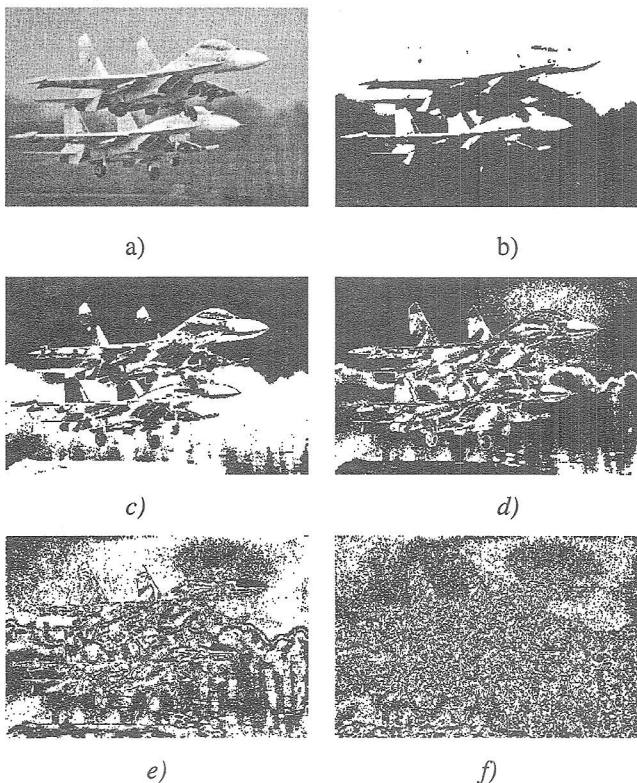


Figure 1. Decomposition of a digital image in bit-planes. a) the original image; b) bit-plane 7; c) bit-plane 6; d) bit-plane 5; e) bit-plane 4; f) bit-plane 3; g) bit-plane 2; h) bit-plane 1; i) bit-plane 0; j) topmost three bit-planes

By observing the images from Figure 1, one can conclude that the bit-planes of greatest weight (i.e. bit-planes 7, 6, 5 and slightly 4) carry most of the information about the image. In other words, on each one of them, separately, it is possible to notice some details from the original image and get an idea about the original picture.

After analyzing the images on Figure 1, it is easy to conclude that the bit-plane 4 carries very little recognizable shapes, but it is still possible to establish some connection between the upper bit-planes and that one. The same goes for the bit-plane 3, though it is harder to establish any obvious connection because the signal turns to noise.

The last three bit-planes, shown on Figure 1g, 1h and 1i) can be practically interpreted as noise. [2]

Having this in mind [1], an attempt was made to reconstruct the bit-planes 4 and 3 from the conditional probabilities evaluated from bit-planes 7, 6 and 5. Thus, it is necessary to make a lossless compression of these bit-planes. It should be noted that bit-planes 7 and 6, shown on Figure 1b and 1c, and sometimes the bit-plane 5, shown on Figure 1d, are composed of big uniform surfaces, which is very suitable for run-length compression.

A few attempts, that were made to calculate the conditional probabilities of bit-planes 4 and 3, will be presented in the next sections.

#### 2.2. Using the three topmost bits as an index for a prediction table for the fourth bit

This is the simplest method for calculating the conditional probabilities. An algorithm in pseudo-code is given in Table 1.

Table 1: Pseudo-code of the algorithm

```

for y = 0 to image_height
  for x = 0 to image_width
    pixel = getPixel(x,y);
    index = pixel.bit7*4+pixel.bit6*2+pixel.bit5*1;
    combination[index]++;
    if pixel.bit4 == 1
      pixel4on[index]++;
    endif
  endfor
endfor
for i = 0 to 7
  probability[index]=pixel4on[index]/combination[index];
endfor

```

This approach in reconstructing the bit-plane 4 is far from being good, because the probability of appearance of the value 0 (or 1) was always close to 0.5, as shown on the Figure 2.

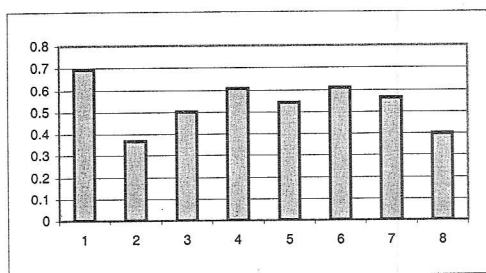


Figure 2: Bar chart of probability of value 1 for bit 4, depending on the bits 7, 6 and 5 of the same pixel.

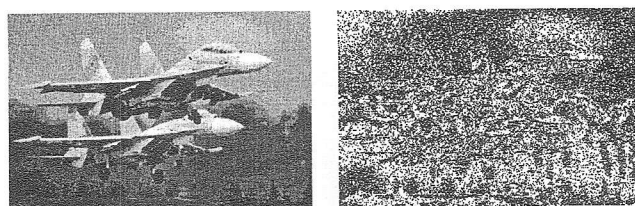
The next step, keeping the same approach in calculating the probabilities, was dividing the image in blocks and applying the same procedure to each of the blocks. Though, this approach did not improve the method: some of the blocks would have a very good reconstruction probabilities, while other blocks still kept the probabilities close to 0.5.

Having in mind that block division did improve the reconstruction probability, another attempt was made to reduce the decision problem in the cases where the probability was close to 0.5. In this attempt, the conditional probability 0 after 1 and 1 after 0 in the bit-plane 4 was calculated. This attempt was not successful either.

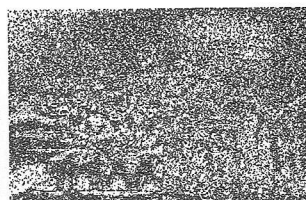
The results of this approach are shown on Figure 3. Block division of 2x2 and 4x4 was used, and the difference from the original image is shown. Only the topmost four bit-planes are included.



a)



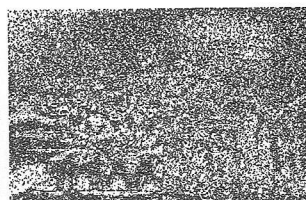
b)



c)



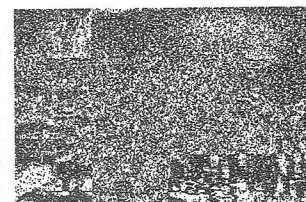
d)



e)



f)



g)

Figure 3. Reconstruction of the image according to the topmost three bits of the given pixel, using block division. a) the original image; b) reconstruction of the image using no block division; c) difference of the reconstructed image and the original; d) reconstruction of the image using 2x2 block division; e) difference of the 2x2 reconstructed image and the original; f) reconstruction of the image using 4x4 block division; g) difference of the 4x4 reconstructed image and the original

It is possible to notice an undesired effect that appears when block division is used on Figure 3f. Very sharp edges between the blocks appear, as the probabilities are calculated for each block separately.

Another undesired effect may also be noticed – the granulation on the reconstructed image, as the intensity of the bit 4 is high enough for a falsely reconstructed bit to appear as a granular noise.

### 2.3. Using the three topmost bits of the given pixel and a few topmost bits of the surrounding pixels as an index for a prediction table for the fourth bit

As shown in the previous section, the topmost three bits are not sufficient for a reliable prediction. An attempt was made to use the topmost three bits of the given pixel as well as a few topmost bits of the surrounding pixels. To be more specific, the surrounding pixels were left, right, above and below the given pixel. Only two topmost bits of the surrounding pixels were used. The algorithm remained the same but the table of the conditional probabilities grew in size from 8 entries to 2048.

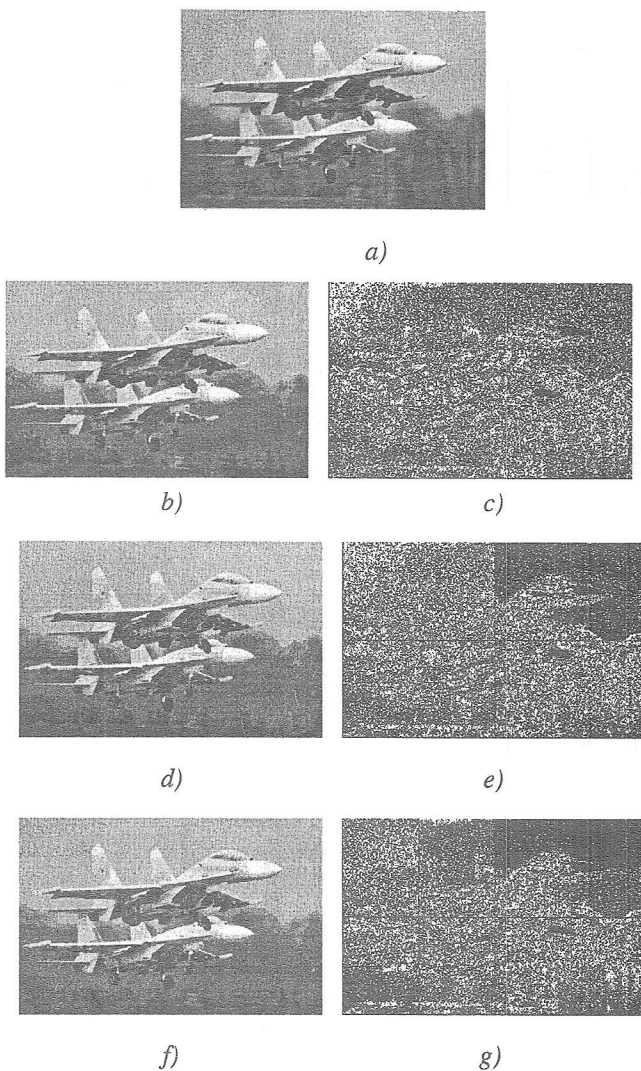


Figure 4. Reconstruction of the image using the topmost bits of the given pixel and the surrounding pixels and block division. a) the original image; b) reconstruction of the image using no block division; c) difference of the reconstructed image and the original; d) reconstruction of the image using 2x2 block division; e) difference of the 2x2 reconstructed image and the original; f) reconstruction of the image using 4x4 block division; g) difference of the 4x4 reconstructed image and the original

The prediction for the bit-plane 3 was done the same way. The results of this approach are shown on Figure 4. With further block division, better results would be achieved, but the compression ratio would be decreased which makes questionable practical application of this method.

Figure 5 gives an overview of the compression ratio depending on the block count. The comparison was made on the original image and the images that were created by transferring bit-planes 7, 6 and 5 with no compression losses, and the probabilities for the bit-planes 4 and 3. The output file was not optimized and only the run length compression for the bit-planes 7, 6 and 5 was used. Finally, the original file in BMP format and the output file were compressed using the ZIP archiving software. The comparison was made on the size of the ZIP archives.

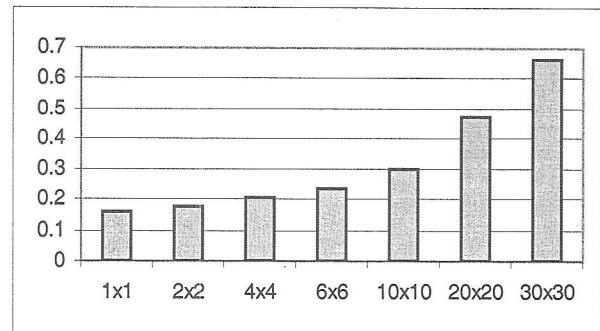


Figure 5: Size ratio between the compressed original image in BMP format and the compressed output file.

On Table 2 is shown an overview of the sizes of the files before and after applying the compression.

Table 2: Overview of the file sizes, before and after applying the compression

	File size [bytes]	ZIP file size [bytes]
BMP	308280	207261
1x1	123800	32702
4x4	198860	42432
10x10	570614	61915
30x30	3945014	137066

Bit-planes 2, 1 and 0 were not taken in consideration in this paper as they have the appearance of noise and therefore the reconstruction of those bit-planes was done by generating random numbers.

The undesirable effects mentioned in the last section are still visible, but the better prediction reduces the effects to a more acceptable level.

The quality of a good image reconstruction could be compared to a 40% JPEG compressed image. Though, in that case, JPEG has a significantly greater level of compression. It should be noted that the output file format used in this paper was not optimized for compression and it could be possible to improve the compression ratio.

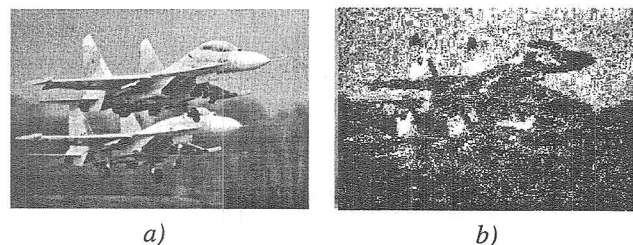


Figure 6: a) JPEG image, 40% quality; b) difference between the original image and the image a)

### 3. CONCLUSION

This paper presents a method of gray-scale digital image compression based on conditional probabilities of appearance of a specific bit value in the bit-planes 4 and 3.

It was shown that the bits 7, 6 and 5 of a given pixel are not a good predictor for bits 4 and 3. A better result is achieved if surrounding pixels are used while a significant improvement is achieved by using block division of the

image. On the other hand, block division reduces the compression ratio.

In further improvement of this method, it would be interesting to use an adaptive block division, with the idea that a block should be divided in 4 sub-blocks (*quad tree*) when the probability of correctly reconstructing the block is below some specified level. That would make this a controllable quality/compression algorithm.

It would also be interesting to find out whether better results would be achieved if more than four surrounding pixels are used.

#### 4. REFERENCES

1. W. Pratt, *Digital Image Processing*, J.W. & Sons, New York, 1978.
2. T. Lončar-Turukalo, V. Crnojević, Ž. Trpovski, *Image Compression by Decomposing into Bit Planes*, TELSIS 2001, 2001.
3. A. Veselinović, D. Dujković, B. Reljin, *Kompresija slike primenom modifikovanog algoritma sa pregrupisavanjem blokova podataka*, ETRAN 2001, 2001.
4. J. Jensen, *Introductory Digital Image Processing*, Prentice-Hall, New Jersey, 1986
5. J. Lim, *Two-dimensional Signal And Image Processing*, Prentice-Hall, 1990.

## A SWITCHING SOURCE OF ARTIFICIAL ELECTROMAGNETIC FIELD FOR GEOPHYSICAL PROSPECTING

Milan Ponjavić, Radivoje Đurić, Faculty of Electrical Engineering, Belgrade, Nenad Smiljanić, Geomagnetic Institute, Grocka

**Abstract:** Audiomagnetotellurics is a specific field in geophysics, which deals with the problem of geological system identification. The system, which is being identified, is a limited volume of the ground to the depth of 1000m that is excited by an artificial periodic electromagnetic field. The sources of the field are specific antennas constructed for magnetotelluric applications. Currents that produce electromagnetic fields are usually in form of periodic narrow pulse trains, with high amplitude, and with frequency from 0.1Hz to 10Hz. For such a shape of current signal, realisation of current generator is complicated as well as the measurement of the response to excitation. A generator, designed as class D power amplifier, is presented in the paper. By using it, current signals of more convenient shape in time domain can be generated, while amplitude spectrum in frequency domain can be programmed to enable accurate identification process.

### 1. INTRODUCTION

Audiomagnetotellurics is a reconstruction technique of the horizontal structure layers of the ground, from surface down to the depth of 1000m, in which artificial electromagnetic field is used as excitation signal.

The technique consists of permanent exposure of the examined volume of ground to a periodic electromagnetic field and simultaneous measurement of electric and magnetic field strength on the Earth surface, above the examined volume, Fig.1.

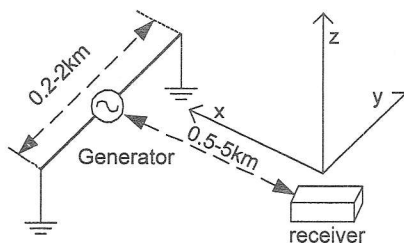


Fig. 1: The system configuration for examination of the Earth layers

The ratio of measured electric and magnetic field gives apparent specific resistance  $\rho(\omega)$ :

$$\rho(\omega) = \frac{2\pi |E_y(j\omega)|^2}{5\omega |H_x(j\omega)|^2} \quad (1)$$

The depth of penetration of an electromagnetic wave into the ground depends on conductance of the Earth layers and on the frequency of the wave itself. By interpreting the equation (1) properly, it is possible to determine dependence of the specific ground resistance upon its depth. It is thereby possible to anticipate the composition of the ground layers on the location where the measurement is performed [1,2].

The source of artificial field can be an antenna in form of current contour laid on the ground, or in form of an grounded dipole – a long conductor whose ends are driven into the ground, and which is coupled in its middle with a generator, as shown in Fig. 1.

Accuracy in determining the dependence of apparent specific resistance upon the depth, relates directly on precision with which the function  $\rho(\omega)$  is determined, which is a common problem in the identification of systems in frequency domain. Thus, the useful frequency range is 0.1 Hz to 1 kHz.

As for any identification problem, it is not only necessary to have quality measurement instrumentation for electrical and magnetic field strength, but also a quality excitation [3]. A generator, which excites an antenna in form of an grounded dipole in the way that a quality identification signal is achieved, is presented in this paper.

### 2. THE CHARACTERISTICS OF THE EXISTING GENERATORS THAT USE AN EARTHED DIPOLE AS AN ANTENNA

Generators used in audiomagnetotellurics are mostly based upon 1kW to 200kW power aggregates [2,4]. Lead acid batteries of great capacity are not so often used. The voltage produced by aggregates is rectified, and in case of batteries, it is increased as to obtain voltage of 500V to 10000V dc. Acquired voltage produces excitation signals, which are brought to the grounded dipole, and which, depending on the resistance between the ends of the dipole, produce the current in time domain of approximately the same shape. The magnetic and electric field on the receiver is directly proportional to the produced current.

According to the kind of signal they produce, the existing generators may be roughly divided into:

- Generators that produce signals with quasi-sine wave voltage form.
- Generators that produce signals in shape of pulse trains.

The signals from the first group are in form of sine wave or of such a pulse train with a poor spectrum and a dominant spectral component on the fundamental frequency [4]. The most frequent example is a rectangular train with 50% duty ratio. Such signals can be represented by the formula:

$$s(t) = s_1(t)(h(t) - h(t - \tau)) \quad (2)$$

where  $s_1(t)$  denotes analytical form of the sine wave or rectangular pulse train:

$$s_1(t) = A_0 \sin(\omega_0 t + \varphi) \quad (3)$$

or

$$s_1(t) = \sum_{k=-\infty}^{+\infty} U_0 (h(t - kT) - h(t - kT - \Delta t)) \quad (4)$$

$h(t)$  is Heaviside's step function, and  $\tau$  is the duration of the generated signal,  $T$  is a period, while  $\Delta t < T$  denotes the

width of a pulse in a train. The measurement of transfer function is reduced to generating of an excitation signal on the frequencies of interest and the measurement of the response. Interpolation of the results gives the function  $\rho(\omega)$ .

Such signals also provide the best signal-to-noise ratio on the receiver and they enable the best reconstruction of the transfer function. A problem in working with them is that the complete measurement must be repeated for every frequency of interest. That means 1000 measurements for a 1Hz resolution in range from 1 Hz to 1000Hz. As the signal  $s(t)$  is aperiodic, its duration should be as long as possible so that its spectrum could more precisely approximate the spectrum of signal  $s_T(t)$ . Because of that, each measurement should last long enough to record a stationary state that practically depends only upon the shape of signal  $s_T(t)$ .

Pulse trains rich in spectrum [4] enable transfer function to be approximately determined by only one measurement. As the transfer function determined in this way may differ considerably from the exact one, sometimes it is necessary to repeat the measurements with signals of quasi-sine form. Measurements should be done around the frequencies where zeros and poles of the transfer function are located. By combining measurements, using the both kinds of signals, it is possible to shorten the duration of the procedure without serious loss of accuracy.

Pulse trains are most often realised in two shapes. The first shape is a rectangular pulse train, where the analytical form of base period is the same as in equation (4), where  $U_0$  denotes pulse amplitude, while  $\Delta t$  denotes its duration.

To obtain a useful spectrum as broad as possible, pulses should be narrow and high in amplitude. Unfortunately, high signal amplitudes are not convenient for practical realisation, and the pulse itself, since it has to be as narrow as possible, does not have high energy. As energy is distributed to all spectral components of a signal, each spectral component does not have high energy. Signal-to-noise ratio is not so good as in the case of quasi-sine signals where the greater amount of energy is concentrated on one spectral component.

By altering the pulse width, the shape of a spectrum can be changed. By broadening the pulse, the width of the useful spectrum is reduced, and energy becomes more concentrated in the part of the spectrum near the fundamental harmonic. A spectrum of a pulse signal of 2000V amplitude, 2s period and 25ms duration is shown on Fig. 2.

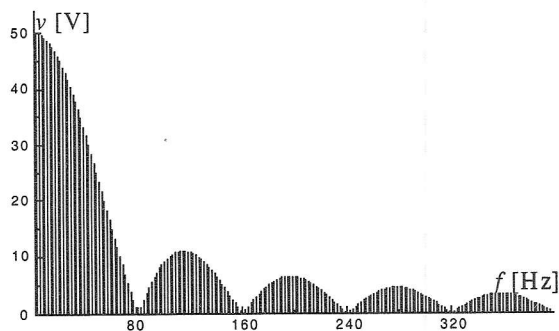


Fig.2. The amplitude spectrum of a pulse signal of 2000V amplitude, 2s period and 25ms duration.

The highest amplitudes of the spectral components are merely 50V while on certain frequencies there are gaps, which have a negative influence upon the identification of the transfer function. For the resistance of  $10\Omega$  between the ends of the grounded dipole, instantaneous value of the current will be 200A, while the value of the largest harmonic current components will be 5A at most. Maximal power for the pulse duration is 400kW, whereas medium power is 5kW.

Another shape consists of signal trains with exponential decreasing pulses. The analytical form of those signals is given by formula:

$$s(t) = \sum_{k=-\infty}^{+\infty} U_0 e^{-\frac{t-kT}{T_0}} (h(t-kT) - h(t-kT-\Delta t)) \quad (5)$$

The working principle of the generator used for producing signals with exponential decreasing pulses [2], is based upon periodical charging of a high voltage capacitor and periodical discharging through the grounded dipole. The time constant  $T_0$  is equal to the product of the resistance between the electrodes and the capacity of the capacitor. The Fig. 3 shows a spectrum of signal, which consists of a train of 0.1Hz frequency pulses obtained by discharging  $50\mu\text{F}$  capacitor charged at 10000V through the ground of  $1000\Omega$  resistance.

Maximal developed power is 100kW, whereas medium power is 0.25kW. Such signals are convenient for high resistance between electrodes.

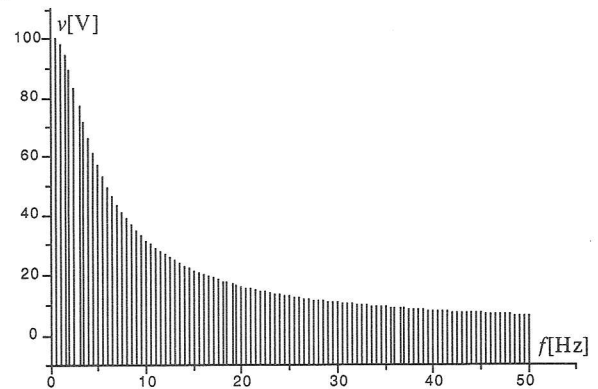


Fig.3: The amplitude spectrum of an exponential decreasing pulse train of 2000V amplitude, 2s period and 25ms duration.

### 3. EXCITATION SIGNALS WITH IMPROVED CHARACTERISTICS

When the excitation signals are in shape of a pulse train, responding signals will have similar shape. Such a signal shape is not convenient for measurement, because the maximal value is high, and most of the time the signal is approximately zero. The resolution of A/D converter in the receiver must cover the whole range of the signal, causing that the low signal values, present in most of the period, are measured with low resolution.

Another problem is that the signal power is concentrated in the short part of the period, while for the longer part of the period the power is equal to zero.

To achieve measurement as efficient as possible, maximal value of the excitation signal in time domain should be made as low as possible, and the amplitude spectrum

should be concentrated on frequencies where zeroes and poles of the identified system are located [6]. Not all spectral components which are on integer multiples of the fundamental need to be present, but only those which are on frequencies of interest. A synthesis of the signals possessing such characteristics is described in [7].

The most convenient signal from this group is the signal in shape of sine waves sum, described by the formula:

$$s(t) = \sum_{n=1}^N A_n \cos(n\omega t + \varphi_n) \quad (5)$$

where  $A_n$  denotes the given amplitude of each harmonic and it can be arbitrary, while  $\varphi_n$  denotes the phase of each harmonic. The phases are so chosen that the amplitude of  $s(t)$  is minimally possible. Fig. 4 shows a period of a signal in shape of sum of sine waves, whose phases are optimised so that its maximal instantaneous value is minimally possible.

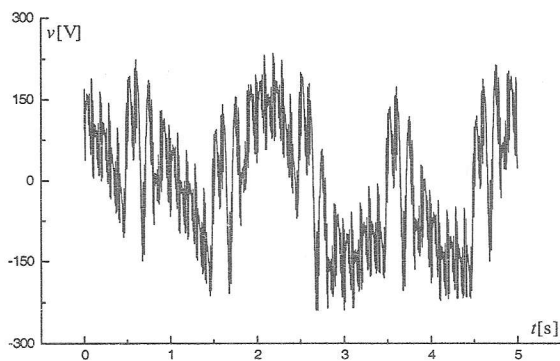


Fig.4. A period of signal in the form of sine waves sum, with optimised phases

The shown signal has the amplitude spectrum represented in Fig. 5. Effective value of the signal is 180V, and its amplitude is 244V.

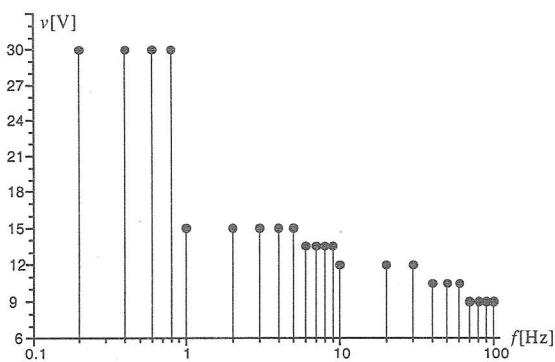


Fig.5: The amplitude spectrum of the signal from Fig. 4.

The power of the signal is artificially distributed across the period and is concentrated only on harmonics of interest. In case of the ground resistance of the 10Ω, the power would be 3.24kW, and the generator need not be oversized. The signal shape in time domain is more convenient than in case of the signals in form of pulse train.

If a signal with "rich" spectrum is needed, it is possible to construct it so that it has an amplitude spectrum equal to any signal of the type of narrow pulse trains, with power distributed across the whole period. The class of those

signals is known as "Maximum Length Binary Sequence" (MLBS). The synthesis of such signals is described in [3]. Fig. 6 shows a period of a signal that has a spectrum similar to the signal from Fig. 2. Fig. 7 shows its amplitude spectrum.

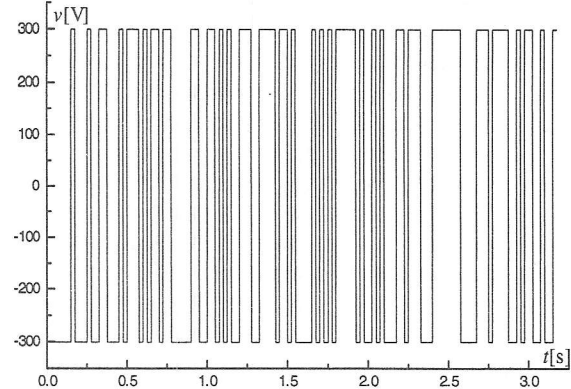


Fig.6: MLBS signal that simulates rectangular pulse

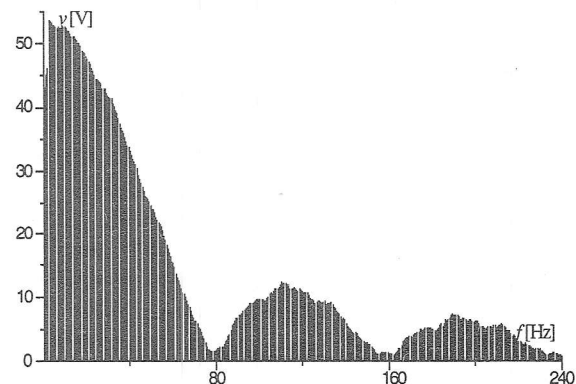


Fig.7: The amplitude spectrum of the signal from Fig. 6.

#### 4. SWITCHING GENERATOR FOR AUDIOMAGNETOLLURICS

Main drawbacks of the existing generators are their inflexibility regarding the programming of the spectrum of signals they should produce. Beside, they often have to be oversized because of the shape of the signals in time domain.

A generator that could overcome the cited disadvantages should be able to produce signals of arbitrary shape in time domain, and also to produce signals with amplitude spectrum defined beforehand.

Fig. 8 shows principal diagram of power part of a generator constructed in form of class D power amplifier, which can generate voltage of arbitrary shape.

Fig. 9 shows block diagram of the control part of the generator.

The power part is designed in form of full bridge, supplied by source of dc voltage. In current realisation source of dc voltage is rectified voltage of 220V/50Hz aggregate with 1.2kW power.

The control part is based on the microcontroller 80C552. Using RS232 interface, one period samples of several different excitation signals are written into NVRAM memory. By using the keyboard, it can be selected which

signal from NVRAM memory is to be brought to D/A converter of the microcontroller, and frequency on which the samples of the chosen signals are written into D/A converter register. The output voltage of D/A converter is compared to 75kHz-frequency ramp and the signal obtained in such a way is used for controlling the bridge transistors.

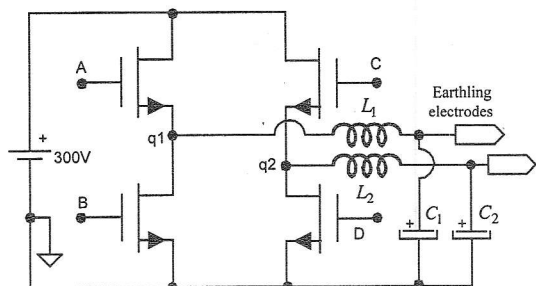


Fig.8: Power electronic part of class D switching generator

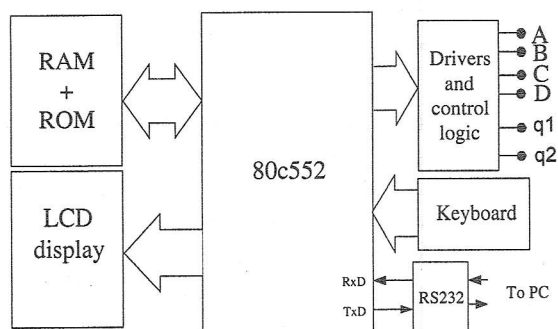


Fig. 9: Digital part of class D switching generator

The generator is tested in laboratory conditions on the variable load with maximal resistance of  $500\Omega$ . Sine wave shape signals, MLBS sequences and multi-sine wave signals have been tested.

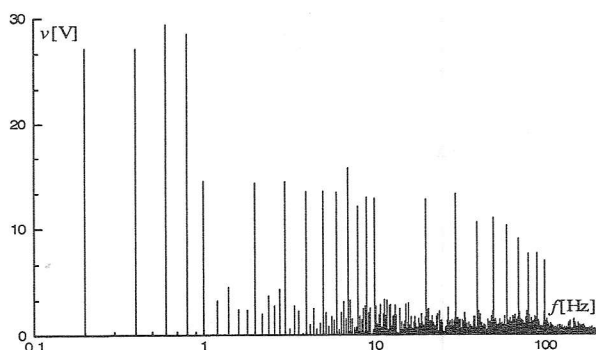


Fig.10: Amplitude spectrum of signal generated upon samples of signal from Fig. 4

Amplitude spectrum of signal from the generator, based on samples of signal from Fig. 4, is shown in fig. 10. The shape in time domain of the signal is impossible to distinguish from the shape of the signal from Fig. 4.

## 5. CONCLUSION

The paper analyses characteristics of a generator of artificial electromagnetic field for audiomagnetotellurics, regarding the power and the harmonic content of generated output signals. Several kinds of signals, already known in the system identification theory in frequency domain, which can replace the signals used until now, are described. The suggested signals with less power have the same or better harmonic content than the signals commonly used. The source, which can generate described signals, is suggested and its realisation is described. The example of harmonic content of multi-sine wave signal produced by the suggested generator is also given.

The power part of the suggested generator is designed as a class D power amplifier, which enables the arbitrary shape of output voltage and therefore the current with harmonic content defined beforehand. The control part of the generator is based on a microcontroller that enables synthesis of a signal of arbitrary harmonic content, which will be amplified by a class D power amplifier.

## 6. REFERENCES

- [1] George V. Keller, Frank C. Frischknecht, *Electrical Methods in Geophysical Prospecting*, Oxford: Pergamon Press, 1966.
- [2] Pierre A. Schegg, "Testing a New Multichannel controlled-source Audiomagnetotelluric Method (CSAMT) on a borehole," *Ecolgae geol. Helv.* 85/2, pp. 459-470, April 1992.
- [3] Johan Soukens, Rik Pintelon, Edwin Van Der Ouderaa, Jean Renneboog, "Survey of Excitation Signals for FFT Based Signal Analyzers," *IEEE Transactions on Instrumentation and Measurement*, Vol 37, no. 3, September 1988.
- [4] J.D.McNeill, "Applications of Transient Electromagnetic Tehniques," *Tehchnical note TN-7*, Ontario, Geonics Limited, 1980.
- [5] "Advanced Electromagnetic Exploration," *Metronics Geometra*, Braunschweig, 1987.
- [6] J. Soukens and R. Pintelon, *Identification of Linear Systems: A Practical Guideline for Accurate Modeling*, London: Pergamon Press, 1991.
- [7] Edwin Van Der Ouderaa, Johan Soukens, Jean Renneboog, "Peak Factor Minimization of Input and Output Signals of Linear Systems," *IEEE Transactions on Instrumentation and Measurement*, Vol 37, no. 2, June 1988.

## CURRENT GAIN FREQUENCY CHARACTERISTICS OF ULTRA-NARROW BASE BIPOLAR TRANSISTORS

Tatjana Pešić, Nebojša Janković, *Faculty of Electronic Engineering, Niš*  
Jugoslav Karamarković, *Faculty of Civil Engineering and Architecture, Niš*

**Abstract** - The current gain magnitude- and phase-frequency characteristics of modern ultra-narrow base bipolar transistors are analyzed in this paper. Using a novel non-quasi-stationary model of bipolar transistors, it is shown that the relaxation time term appearing in Boltzmann transport equations, has substantial influence on current gain frequency characteristics at high frequencies. It is also shown that this influence increases with base width shrinkage and with increase of base-emitter voltage.

### 1. INTRODUCTION

The optimized structures of modern integrated bipolar transistors with polysilicon emitter and/or ultra-narrow SiGe base reach the cut-off frequencies  $f_t$  ( $f_t$  is frequency where magnitude of current gain  $\beta$  is unity) higher than 100 GHz [1]. Experimental determination of  $f_t$  at such high frequencies has high technical demands and often experiences difficulties. Thus, the determination of  $f_t$  consists of recording the measurements points up to experimental limits, and extrapolation of current gain magnitude-frequency characteristic with a  $-20$  dB/dec line, following the standard model of BJT frequency response [1,2]. An example of practical determination of  $f_t$  for the SiGe HBT with base width  $W_b = 50$  nm is shown in Fig. 1 [1].

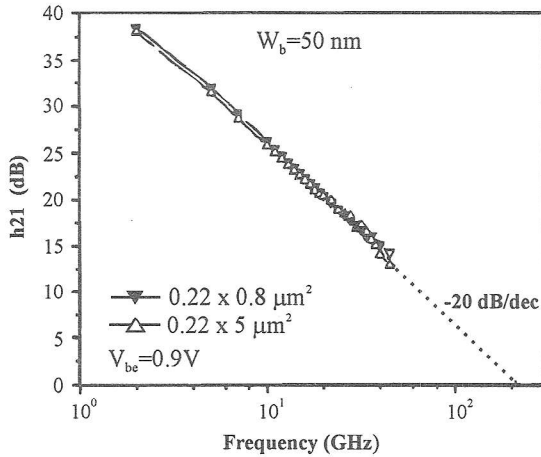


Fig.1. An example of  $f_t$  determination for the ultra-narrow base bipolar transistors by the extrapolation [1].

The knowledge of  $f_t$  exact value is very important since it is used for adjustment of electrical model parameters of BJT in circuit simulators (e.g. SPICE). The aim of this paper is to show theoretically that in modern BJT with very narrow bases described procedure for  $f_t$  determination may not be applicable.

### 2. ULTRA-NARROW BASE BJT MODEL

1D transport through quasi-neutral regions of BJT in arbitrary injection level can be described with the system of partial differential equations [3]:

$$-\frac{\partial u}{\partial x} = \frac{p}{kT\mu_n n_{ie}^2} \left( J + \tau \frac{\partial J}{\partial t} \right), \quad (1)$$

$$-\frac{\partial J}{\partial x} = q \frac{p_0 n_0}{p+n} \frac{\partial u}{\partial t} + u q n_{ie}^2 \left\{ C_n n + C_p p + \frac{1}{\tau_{p0}(n+n_{ie}) + \tau_{p0}(p+n_{ie})} \right\}, \quad (2)$$

where the system variables are:

$$j(x,t) = -j_n(x,t), \quad (3)$$

$$u(x,t) = \frac{p(x,t)n(x,t) - n_{ie}^2(x)}{n_{ie}^2(x)}. \quad (4)$$

where  $j_n(x,t)$  being minority electron current density in the base (in the case of npn transistor). This system of partial differential equations (1)-(2) is fully analogous to telegraphers' equations written for the equivalent non-linear inhomogeneous lossy transmission line (TL):

$$-\frac{\partial u(x,t)}{\partial x} = \left[ R'(x,u) + L'(x,u) \frac{\partial}{\partial t} \right] j(x,t), \quad (5)$$

$$-\frac{\partial j(x,t)}{\partial x} = \left[ G'(x,u) + C'(x,u) \frac{\partial}{\partial t} \right] u(x,t). \quad (6)$$

Following (1)-(2), parameters of equivalent TL,  $R'$ ,  $L'$ ,  $G'$ , and  $C'$ , can be expressed as [3]:

$$R'(x,u) = \frac{p(x,u)}{kT\mu_n(x)n_{ie}^2(x)}, \quad (7)$$

$$L'(x,u) = \frac{m_n^* p(x,u)}{qkTn_{ie}^2(x)}, \quad (8)$$

$$G'(x,u) = q n_{ie}^2(x) \left\{ C_n n(x,u) + C_p p(x,u) + \frac{1}{\tau_{p0}(n(x,u) + n_{ie}(x)) + \tau_{n0}(p(x,u) + n_{ie}(x))} \right\}, \quad (9)$$

$$C'(x,u) = q \frac{n_{ie}^2(x)}{p(x,u) + n(x,u)}. \quad (10)$$

In comparison with the classical transport models, the difference of this approach is appearance of the term  $\tau(\partial J/\partial t)$  in eqn. (1). It follows from the exact solution of Boltzmann transport equation in relaxation time approximation [4] and corresponds to the inductance per unit length  $L'(x,u)$  in the equivalent TL model.

Modeling the minority carrier transport with TL approach, a novel 1D non-quasi-static (NQS) BJT model for

the application in circuit simulators has been developed [5]. For the first time in the literature it included the diffusion inductance, introduced through the relaxation time term in Boltzmann transport equation. We have recently shown that  $L'(x,u)$  influences distortion of output signals and time delay in transistors with very narrow bases [6,7].

The results obtained by novel NQS model presented in this paper shows that inductive term influences also high frequency region of ultra-narrow bases transistors AC frequency characteristics, especially in the case of high injection level.

**3. RESULTS AND DISCUSSION**

Using the novel NQS model, the magnitude- and phase-frequency characteristics of the common emitter current gain have been numerically calculated for different widths of quasi-neutral regions. In these calculations all other transistor parameters (such as the width of emitter and collector regions, as well as maximum and minimum concentration in the base region) have been kept constant.

Fig. 2 shows 1D profile for two transistor structures with different base QNR widths.

Fig. 3 shows magnitude- and phase-frequency characteristics of current gain, calculated with and without inclusion of inductive term  $L'$  in NQS model in the case of low injection level ( $V_{be} = 0.6V$ ). It can be seen that diffusion inductivity practically does not influence characteristics of transistor with wider base  $W_b = 300$  nm, while only the slight disturbance in the vicinity of cut-off frequency is occurred for transistor with narrower base ( $W_b = 50$  nm).

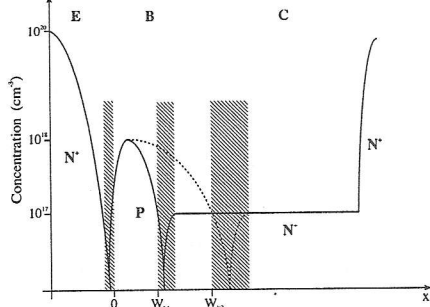
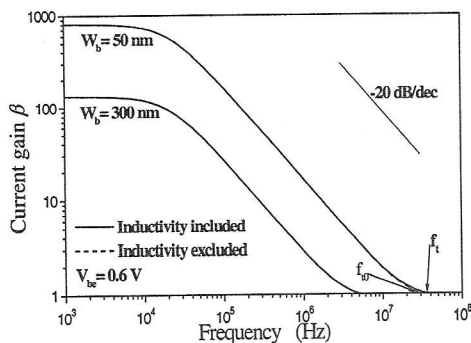
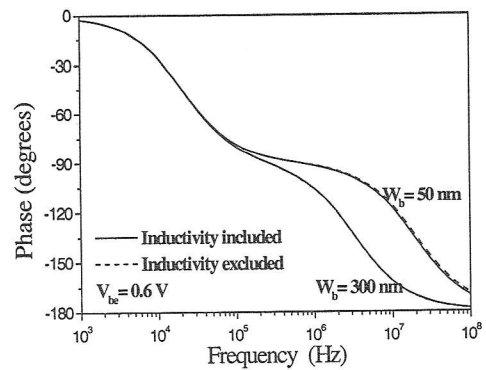


Fig.2. Illustration of analyzed transistor profiles with different base QNR widths. The marked areas correspond to space-charge regions.

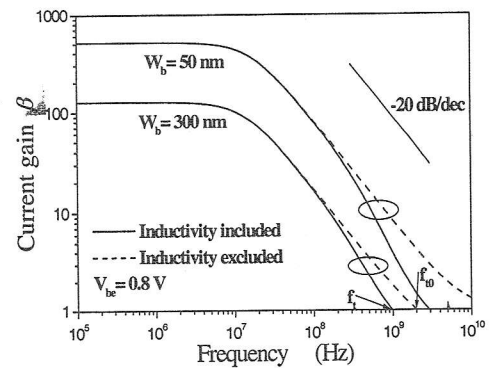


(a)

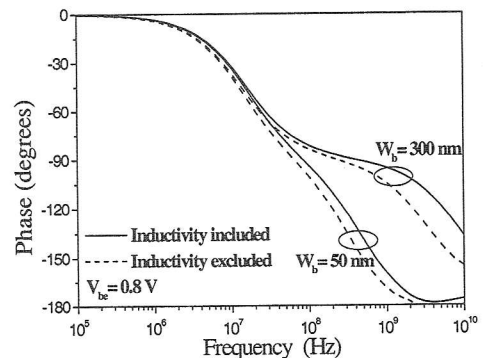


(b)

Fig.3. Magnitude- (a) and phase- (b) frequency characteristics of current gain with and without inductivity parameter  $L'$  for two different base QNR widths.



(a)



(b)

Fig.4. Magnitude- (a) and phase- (b) frequency characteristics of current gain with and without inductivity parameter  $L'$  for two different base QNR widths for  $V_{be}$  yielding maximum  $f_i$ .

Fig. 4 shows magnitude- and phase-frequency characteristics of current gain for moderate injection level ( $V_{be} = 0.8V$ ). The  $V_{be}$  value has been chosen as the value that gives maximum in  $f_t(I_c)$  characteristic, i.e. it represents the operating point where transistor is the fastest. Fig. 4 also shows significant difference of magnitude- and phase-frequency characteristics obtained with inclusion of  $L'$  comparing to characteristics with  $L'$  excluded. This difference is bigger in the case of transistor with narrower base ( $W_b = 50$  nm). The decrease of  $\beta$  magnitude at higher frequencies starts to differ from theoretical slope of  $-20$  db/dec, resulting in lower value of cut-off frequency ( $f_t$  instead of theoretical  $f_{t0}$ ). Such behavior implies existence of additional effective zeros and poles in transfer function of transistors with ultra-narrow bases that appear for higher frequencies. This modification of  $\beta$  is important since the linear extrapolation method for estimation of  $f_t$  now gives fictive cut-off frequency value  $f_{t0}$  higher than real  $f_t$ . Thus, linear extrapolation method in the case of ultra-narrow bases becomes questionable.

Also, Fig. 4.b. shows significant difference in estimation of current gain phase at high frequencies if  $L'$  is excluded. This is very important in the case of wide-band amplifiers where exact modeling of transistor phase-frequency characteristic plays very significant role. Thus, the application of novel NQS BJT model in a circuit simulator could lead to much more precise determination of the transistor frequency characteristics.

Fig. 5 shows relative error of cut-off frequency  $(f_t - f_{t0})/f_t$ , expressed in percentage, obtained with NQS BJT model with and without inductive term  $L'$ , for different values of base QNR width  $W_b$ . It can be seen that error rapidly increases with the decrease of  $W_b$  and that error is bigger for higher level of injection (i.e. base-emitter voltage). The analysis hasn't been done for  $W_b$  lower than 50 nm since in that region quasi-ballistic effects [8], which are not included in the model, start to dominate.

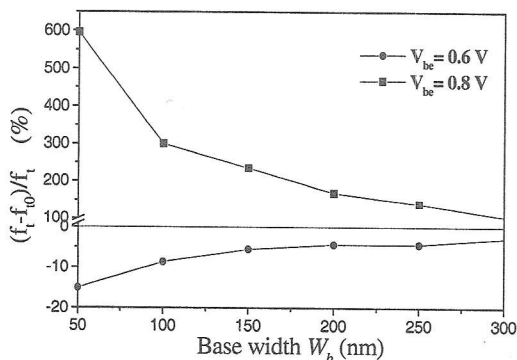


Fig.5. Relative error in extrapolation method for cut-off frequency estimation vs. base QNR widths for low and moderate injection levels.

#### 4. CONSLUSION

A transmission line based non-quasi-static BJT model has been applied in the modeling of current gain frequency characteristics for transistors with ultra-narrow bases. The model includes relaxation time term from Boltzmann transport equation. The obtained results show that this term induces the disturbance of magnitude-frequency characteristic from theoretical gradient of  $-20$  db/dec. This disturbance appears in the vicinity of cut-off frequency and increases with base width shrinkage. It may lead to incorrect estimation of experimental cut-off frequency  $f_t$ . The relaxation time term has also significant influence on current gain phase-frequency characteristic, which has to be taken into account in simulation of stability of wide-band amplifiers and other similar integrated circuits with modern bipolar transistors.

#### 5. REFERENCES

- [1] S.J. Jeng, B. Jagannathan, J.-S. Rieh, J. Johnson, K.T. Schonenberg, D. Greenberg, A. Stricker, H. Chen, M. Khater, D. Ahlgren, G. Freeman, K. Stein, S. Subbanna, "A 210-GHz  $f_T$  SiGe HBT with a Non-Self-Aligned Structure", *IEEE Electron Device Letters*, vol. 22, pp. 542-544, November 2001.
- [2] K. Jenkins, "Frequency Response of Advanced Silicon Bipolar Transistors at Low Temperatures", *IEEE Trans. on Electron Devices*, vol. 37, pp. 2243-2249, October 1990.
- [3] T. Pesic, T. Ilic, N. Jankovic, J. Karamarkovic, "Transient analysis of BJT using all injection level TLEC model", *Proc. of 22<sup>nd</sup> International Conference on Microelectronics MIEL 2000*, vol. 1, pp. 149-152, Nis, Yugoslavia, 2000.
- [4] S. Selberherr, W. Griebel, H. Potzl, "Transport physics for modeling semiconductor devices", *Proc. of International Conference on Simulation of Semiconductor Devices and Processes*, Swansea, UK, pp. 133-152, 1984.
- [5] N. Jankovic, T. Pesic, J. Karamarkovic, "1D Physically Based Non-Quasi-Static Analog Behavioral BJT Model for SPICE", *Proc. of 23<sup>rd</sup> International Conference on Microelectronics - MIEL 2002*, vol. 2, pp. 463-468, Nis, 2002.
- [6] J.P. Karamarkovic, N.D. Jankovic, B.D. Milovanovic, "Periodical Steady-State Analysis of Minority Carrier Diffusion including Momentum Relaxation Time", *Electronics Letters*, vol. 29, pp. 1316-1317, 1993.
- [7] J.P. Karamarkovic, N.D. Jankovic, D.B. Glozic, "Transmission Line Equivalent Circuit Model of Minority Carrier Transient Current in Quasi-Neutral Silicon Layers including Inductive Effect", *International Journal of Numerical Modelling - Electronic Networks, Devices and Fields*, vol. 8, pp. 341-356, 1995.
- [8] J. Karamarkovic, N. Jankovic, "Modification of Drift-diffusion Model for Short Base Transport", *IEE Electronic Letters*, Vol.36 No.36, pp.2047-2049, 2000.

## ACTIVE MICROWAVE MULTIPLIERS AT X BAND

Darko Radulović, Aleksandar Nešić, *Institute for Microwave Technique and Electronics in Belgrade*

**Abstract** - In this paper is described concept, analysis and realization of microwave frequency multiplier with factor 8 for frequency band between 10 and 12 GHz. First stage works as doubler and it is designed with lumped elements in input circuit of BJT. Second stage, multiplies frequency of input signal four times and it is designed in microstrip technique. It is realized as balanced configuration of two HEMTs (NE3210S01). Total attenuation of designed frequency multiplying chain is about 2 dB. Each stage is first realized as independent circuit, and later both stages are integrated in one circuit. Integration additionally increases total gain of multiplying chain, because in integrated configuration we need only one matching circuit between stages.

**Keywords** - Frequency Multiplying, Active Microwave Circuits, Balanced Configuration of HEMTs, Harmonic Balance Analysis.

### 1. INTRODUCTION

In microwave communication systems large part of electronic devices is used for generation of signals with required frequencies. Most common way to generate signal, which has high frequency, is by multiplying chain. First stage in multiplying chain is generator of frequency of fundamental harmonic (about 100 MHz) from very stable source such as crystal oscillator. Second stage is generator of harmonic of higher order, which is equal to required high frequency. Signals, which are obtained in this way, are very stable and with very low noise level. Obviously, for generation of required harmonic, nonlinear circuits have to be used.

Most commonly used nonlinear elements in multiplying circuits are diodes (varactor, step-recovery, Schottky-barrier). In last few years FET frequency multipliers are becoming more dominant compare to diode multipliers because of their numerous advantages. FET multipliers have broader bandwidths, as well as gain of conversion higher than one. Also, multiplying chains with FETs are dissipating less heat and less power of supply is required for their realization; this is important advantage in systems such as wireless LAN network, different mobile and fixed microwave telecommunication systems, etc.

### 2. DESIGN OVERVIEW

Main task of design of multipliers in this paper was to achieve as high as possible gain of circuit for required frequency bandwidth at the output. Required attenuation of non-desirable harmonics at the output compare to generated signal is higher than 40 dB. Required 3-dB bandwidth is from 1.39 GHz to 1.44 GHz at the input, or from 11.12 GHz to 11.52 GHz at the output (factor of multiplication is 8, and output bandwidth is  $B=400$  MHz, or  $\pm 2\%$ ).

Solution of the problem is divided in two parts. First is designed doubler which is converting signal which has frequency about 1.4 GHz at the input to signal which has frequency about 2.8 GHz at the output. Then is designed

frequency multiplier with factor 4 (quatriplier) which is converting signal which has frequency of 2.8 GHz at the input to signal which has frequency of 11.2 GHz at the output. Doubler has gain of 3 dB in required bandwidth and quatriplier has attenuation of about 5 dB. This means that designed multiplying chain should have attenuation of about 2 dB.

### 3. THEORETICAL BACKGROUNDS

#### 3.1. Harmonic-balance analysis

For analysis and optimization of frequency multipliers in this paper is used method of Harmonic-Balance (HB) analysis, or more precisely HB Large-Signal Single Tone Analysis.

First step in this method is division of nonlinear circuit on linear and nonlinear part as in Figure 1. Linear part of circuit is then solved in frequency domain and nonlinear part in time domain. Let the voltages at the ports be represented with the complex vectors:  $V_1, \dots, V_N$  and we will presume that these vectors have initial values:

$$V_i = \begin{bmatrix} V_{i0} \\ V_{i1} \\ \dots \\ V_{ik} \end{bmatrix}, \quad i=1, \dots, N \quad (1)$$

where  $V_{i0}, V_{i1}, \dots, V_{ik}$  are complex representatives of harmonics of voltage at port  $i$ . Next step in algorithm is to solve linear part of circuit and to get vector of currents at the ports which correspond to linear part of the network:  $I_1, \dots, I_N$ . Then we will transform these values in time domain and observe these as currents at the inputs of nonlinear part of network. From the characteristics of nonlinear elements we now obtain voltage at the ports, which correspond to nonlinear part of the network:  $\hat{v}_1(t), \dots, \hat{v}_N(t)$  and after frequency transformation we obtain their complex representatives:  $\hat{V}_1, \dots, \hat{V}_N$ . These voltages now should be taken as new initial values for solving of linear part of the network. Method is iteratively repeated until we get satisfying coincidence between vectors  $V_1, \dots, V_N$  and vectors  $\hat{V}_1, \dots, \hat{V}_N$ .

Essence of HB analysis is solution of system of nonlinear equations. There are numerous methods for solving system of nonlinear equations obtained by HB analysis such as: optimization, splitting methods, Newton's method and reflection algorithm. In this paper Newton's method is used and this is actually well known algorithm of numerical mathematics for solving the system of nonlinear equations. For analysis and optimization of multipliers in this paper is used computer program MicroWave Office. This program has implemented described method of HB analysis and corresponded system of equations is solved by Newton's method.

For additional details about method of HB analysis reference [1] is recommended.

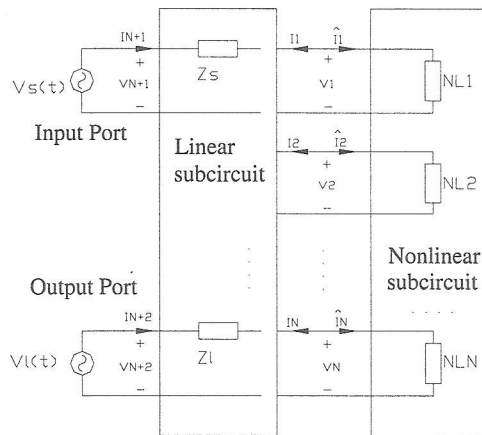


Figure 1. Division of circuit on linear and nonlinear part, in HB analysis method.

### 3.2. Circuit's principle of work

First stage in multiplying chain is realized with bipolar transistors and it is typical example of frequency multiplier with one active element. Layout of the circuit is shown in Figure 1. Active element (which works in class B) is excited with frequency of fundamental harmonic. At the output are notch filters (band-stop), which are set on first, third and fourth harmonic respectively. These filters are also known as traps for corresponded harmonics. Trap for first harmonic is realized with lumped elements and traps for third and fourth harmonics are realized in microstrip technique. Also, input matching network is realized with lumped elements and output matching network is realized in microstrip technique.

Second stage of multiplier is realized with two FET transistors, which are creating balanced configuration. Layout of this circuit is shown in Figure 2b. FETs, which are used, are NEC - NE3210S01. Transistors are working in class B. Gates of transistors are supplied with excitation signal (from the same excitation port) and phase angle between signals at the gates is  $180^\circ$ . Result of excitation of transistors in this way is that they are conducting alternately some time during the one period of excitation signal. Because of this, signal at drain (drains of both transistors are connected in the same point) will be rich with even harmonics, while odd harmonics will be significantly less, including frequency of excitation signal (1st harmonic). Next stage in multiplier is output bandpass filter. It is connected in series with drain. Main task of this filter is to suppress as much as it is possible second harmonic, because this frequency component has very high level at input point of the filter.

### 4. CIRCUIT DESCRIPTION

Layouts of designed circuits are shown in Figures 2a and 2b. Circuits are made on substrate Rogers 4003, which has characteristics:  $\epsilon_r = 3.38$ ,  $\tan \delta = 15 \div 20 \cdot 10^{-4}$ , thickness  $h = 0.2$  mm and metalization thickness  $t = 17$   $\mu\text{m}$ . Bipolar transistor which is used in first stage is Philips BFR 93A, [2], and in second stage HEMT transistors NEC NE 3210S01 are used.

In second stage parallelly to the gates resistors of 200  $\Omega$  are connected. It is done to make easier realization of input matching of multiplier. This certainly resulted in some gain loss, but frequency bandwidth of circuit is increased due to more qualitative realization of input matching.

For modeling of bipolar transistor in computer simulations it is used model proposed from its manufacturer and this model is built in program MicroWave Office. For modeling of FET is used TOM-1 model. Manufacturer gives parameters for this model in catalogue. Additional information about this model can be found in reference [3].

### 5. RESULTS OF MEASUREMENTS AND SIMULATIONS

In this paragraph are given results of measurements and simulations and adequate comparisons are done.

In Figure 3 are given results of measurements of gain of designed doubler, as well as corresponded results of simulations. During the design excitation is fixed at level of 10 dBm, and then optimization of circuit is done, so that the circuit has as high as possible gain. Realized circuit has maximal gain at the excitation level of 14 dBm. When we apply excitation of 14 dBm in computer simulation we obtain that doubler has attenuation of 0.5 dB. Maximal gain of realized circuit is about 3 dB in frequency bandwidth from 1.39 GHz till 1.42 GHz, while the gain of the circuit in the same bandwidth is about 1.5 dB according to computer simulations. In Figure 4 are given results of measurements of power of fourth harmonic at the output of designed frequency multiplier with factor 4. In the same figure are given results obtained by computer simulations. During the design of circuit excitation level was fixed on 8 dBm, and in the process of optimization is obtained that optimal value of gate bias voltage is -0.58 V (when this voltage is applied in circuit we obtain highest possible gain). The same gate bias voltage is optimal for real circuit when excitation level is 8 dBm. Obtained 3 dB-bandwidth of real circuit is from 10.5 GHz to 10.8 GHz.

Undesirable harmonics (first, second, third, fifth and sixth) at the output of four times multiplier are suppressed more than 50 dB. It is achieved by sixth order output bandpass filter, which has high attenuation outside its passband. At the same time this filter has a little bit higher attenuation and ripple inside its passband compare to filters of lower order. On the other hand filters of lower order have lower attenuation outside their passband, so although by their application multiplier would have higher gain, undesirable harmonics at the output would be higher.

During the realization of output bandpass filter of four times frequency multiplier following procedure is applied. First step was initial design of filter according to procedure described in reference [4]. This filter was then analyzed in program MicroWave Office, where additional optimization of filter was done. Characteristic of filter achieved with this procedure was given in Figure 5.

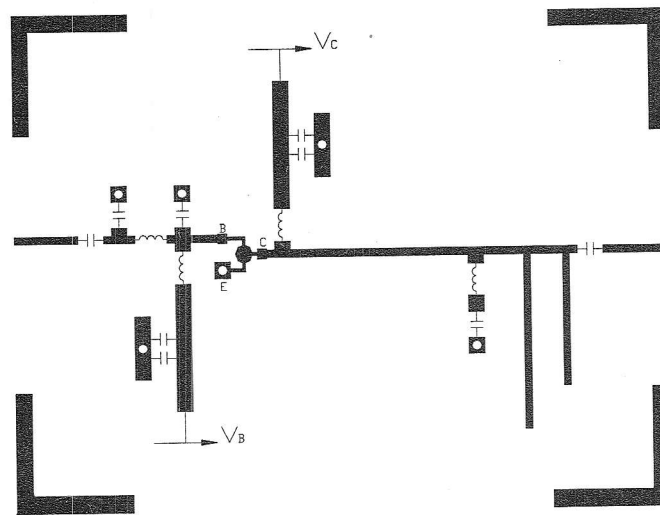


Figure 2a. Layout of designed doubler.

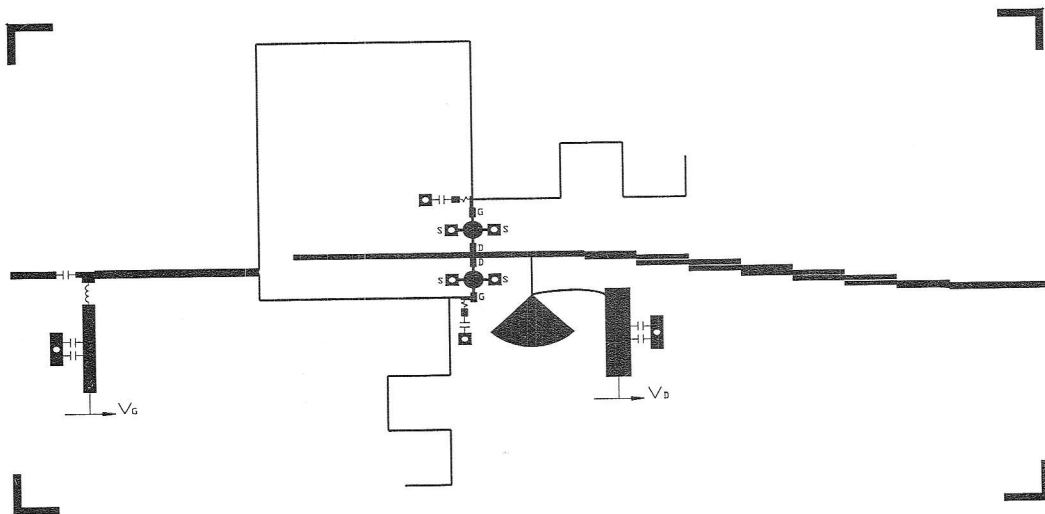


Figure 2b. Layout of designed frequency multiplier with factor 4.

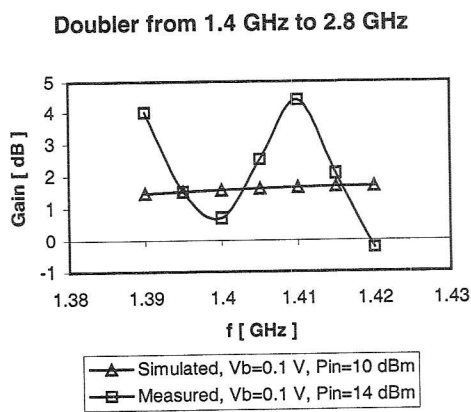


Figure 3. Optimal results of gain of doubler obtained by measurements and simulations when bias base voltage is 0.1 V (optimal value) and when optimal input power level is applied. Achieved level of gain is maximal.

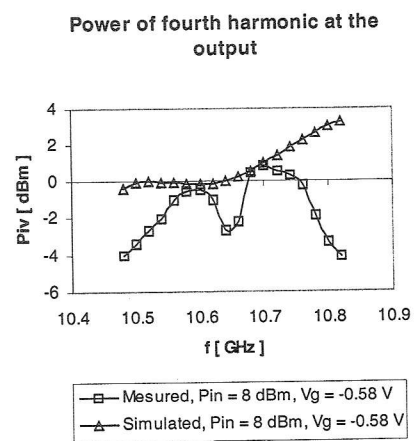


Figure 4. Results of measurements and simulations of power of fourth harmonic at the output of four times frequency multiplier. Excitation power level is fixed at the level of 8 dBm, and gate bias voltage is -0.58 V (optimal values when maximal gain is achieved).

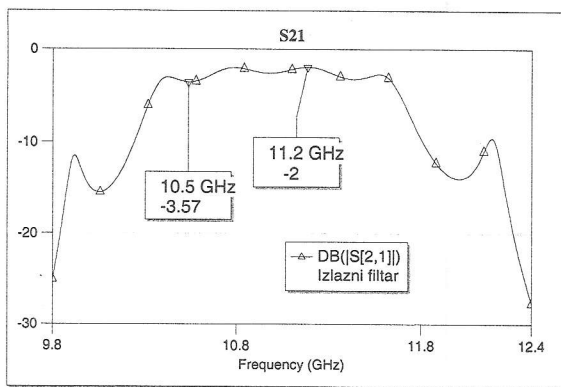


Figure 5. Frequency characteristic of output bandpass filter obtained by analysis in program MicroWave Office.4

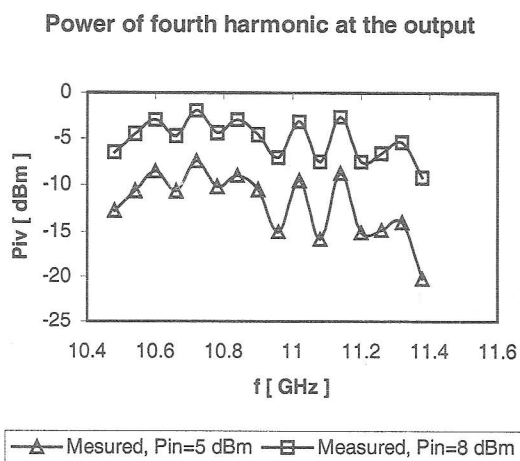


Figure 6. Power of fourth harmonic at the output, when different levels of excitation power are applied. Wider frequency bandwidth is observed. This figure illustrates higher ripple of frequency characteristic of output filter.

In Figure 5 we can see that 3-dB bandwidth of filter is from 10.6 GHz to 11.7 GHz, passband attenuation is about 2 dB and ripple is about 1.6 dB. In Figure 6 are given results of measurements in wider frequency bandwidth around desirable central frequency of 11.2 GHz and when two different levels of excitation power are applied, 5 dBm and 8 dBm. Obviously realized filter has pretty much higher ripple (about 5 dB) and it can't be used around desirable central frequency. Main reason for this is that critical gaps in filter (first and last) which should be 70  $\mu\text{m}$  wide are realized with tolerance from 60  $\mu\text{m}$  to 100  $\mu\text{m}$  (more than 40 %). So, dominant influence on output characteristic of four times frequency multiplier has this filter. Attenuation and ripple can be reduced by filter of lower order, but this will result in decreased attenuation of undesirable harmonics at the output, so adequate trade-off should be done in order to achieve desired characteristics.

In Figure 7 is shown output power level as a function of input power level, at frequency of 10.7 GHz. At this frequency is achieved highest gain of four times frequency

multiplier in its passband. In figure are shown results of measurements and simulations.

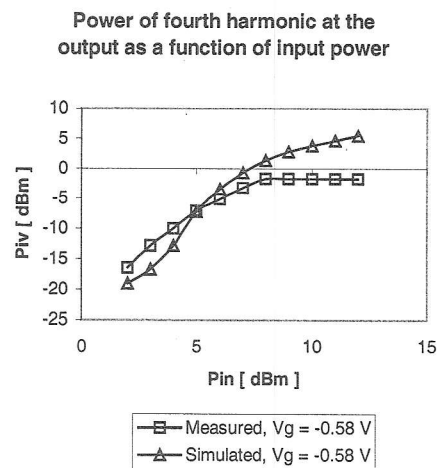


Figure 7. Power of fourth harmonic at the output of four times frequency multiplier as a function of input power. Frequency is fixed at 10.7 GHz (at the output) and gate bias voltage is set to optimal  $V_g = -0.58$  V.

## 6. CONCLUSION

In this paper are verified basic concepts of design of active microwave multipliers at X band. Photolithographic procedure resulted with unexpectedly high errors, so for example tolerance of critical gaps of output bandpass filter in four times frequency multiplier is higher than 40 %. In spite of very high tolerance in dimensions of realized circuits we can say that good agreement of calculations, simulations and experimental results is achieved. Also, we can conclude that models of transistors, which are used in this paper, are suitable for applications in computer simulations of frequency multipliers.

In this paper are presented two single circuits of frequency multipliers (doubler and four times frequency multiplier) and their integration in one circuit, which will be eight times frequency multiplier, is under way.

## 7. REFERENCES

- [1] S. A. Maas, *Nonlinear Microwave Circuits*, Artech House, 1988.
- [2] Philips Semiconductors, *RF Wideband Transistors, Video Transistors and Modules*, 1993.
- [3] A. J. McCamanat, G. D. Cormack, D. H. Smith, "An Improved GaAs MESFET Model for Spice", *IEEE Trans. Microwave Theory Tech.* vol. 38, pp 822-824, June 1990.
- [4] T. C. Edwards, *Foundations for Microstrip Circuit Design*, John Wiley & Sons, 1983.

## ACKNOWLEDGEMENTS

The authors would like to thank Ministry of Science, Technology and Development of Government of Republic of Serbia, which took part in finance of this project, as well as Momčilo Tasić and Milka Marjanović who helped with the fabrication.

## PREPARATION OF ACTIVATED CARBONS BY NaOH

Nikola Nikačević, *Tehološko-Metalurški fakultet, Univerzitet u Beogradu* ;  
Encarnacion Raymundo-Pinero, *Department for Inorganic Chemistry, University of Alicante, Spain*

**Abstract:** Preparation of activated carbons by chemical activation with NaOH. Row material was Spanish anthracite and preparation method was physical mixing. Method for detecting surface oxygen groups was temperature programmed desorption (TPD). Porous texture of activated carbons has been characterised using physical adsorption of  $N_2$  at 77K and  $CO_2$  at 273K. Influence of different activated agent to coal ratio on pore texture was studied.

**Keywords:** Activated carbon, Chemical activation by NaOH, Surface groups, Microporous texture

### 1. INTRODUCTION

Activated carbon are widely used as adsorbent in technologies related to pollution abatement due to their highly porous texture and large adsorption capacity [1-3]. However, controlled pore size and pore size distribution are necessary for the application of those materials in a specific end use. Basically, there are two different processes for the preparation of activated carbons, so-called physical and chemical activation. Physical activation involves carbonization of a carbonaceous precursor followed by gasification of the resulting char or direct activation of the starting material in the presence of an activating agent such as  $CO_2$ , steam or a combination of both [4,5]. In chemical activation the precursor is impregnated with a given chemical agent and, after that, is pyrolyzed. As a result of the pyrolysis process a much richer carbon content material with a much more ordered structure is produced, and once the chemical agent is eliminated after the heat treatment, the porosity is much more developed [6]. Several activated agents have been reported for the chemical activation process: phosphoric acid, zinc chloride and alkaline metal compounds. Phosphoric acid and zinc chloride are activated agents usually used for the activation of lignocellulosic materials which have not previously carbonized [7,8]. Alkaline metal compounds, usually KOH, are used for the activation of coal chars [6,9].

This paper is analysing the development of porosity of a Spanish anthracite by chemical activation with NaOH. Preparation method is physical mixing of NaOH and coal, which is a very easy method and renders the best results.

Research was done at the Department for Inorganic Chemistry, University of Alicante, Spain.

### 2. EXPERIMENTAL

Row material was anthracite Galletilla from Spanish mines. The preparation method was physical mixing (solid phase). Activated agent was NaOH (Aldrich 97%). Weigh of carbon was 14g. Different activated agent to carbon ratio have been tested: 1/1, 2/1, 3/1, 4/1, 6/1. The nomenclature includes ACNa (chemical activation by NaOH) and activated agent/coal ratio (ACNa1, ACNa2, ACNa3, ACNa4, ACNa6).

The reactor was furnace constructed by the Department of Inorganic Chemistry, Univ. Alicante, and control system was Eurotherm Controls. Flow rate of  $N_2$  was

3000 ml/min. Heating rate was  $5^\circ C/min$  up to maximum temperature of  $730^\circ C$ , and then has been held at that temperature for one hour. The sample was left in the furnace over night (low flow rate of  $N_2$ ).

The following step was washing in the 5M HCl (500 cl). The procedure was repeated 5 times (one day each washing) until the colour of the filtration liquid was transparent (all mineral matter removed). Then chlorine ions were washed by pure water ( $< 50 \mu S$ , 500 cl).

Temperature programmed desorption (TPD) in inert atmosphere ( $N_2$  flow rate was 705 ml/min) was performed in order to analyse surface chemistry of activated carbons. Vertical differential flow reactor (1,2 cm diameter) with sample was placed in the furnace and was heated up to  $900^\circ C$  with the heat rate of  $20^\circ C/min$ . Outlet of gases was analysed by IR and UV analysers (Fisher-Rosemount BINOS 100 for  $CO/CO_2$ ). The concentrations of the  $CO$  and  $CO_2$  on the outlet were recorded every 10 seconds.

Porous texture of activated carbons has been characterised using physical adsorption of  $N_2$  at 77K and  $CO_2$  at 273K in Autosorb-6 apparatus.

### 3. RESULTS AND DISCUSSION

Oxygen groups are present at the surface of activated carbons. Such groups may be important for specific end use. They can physically block pores or active sites and thus limit adsorption or catalytic reaction. Also, oxygen groups can attract or reject substances depending on chemical properties.

The method used for detecting surface groups was temperature programmed desorption (TPD). Surface oxygen groups decompose upon heating by realising  $CO$  and  $CO_2$  on different temperatures. Fig. 1. shows the evolution of the  $CO$  and  $CO_2$  at different temperatures for carbon ACNa3.

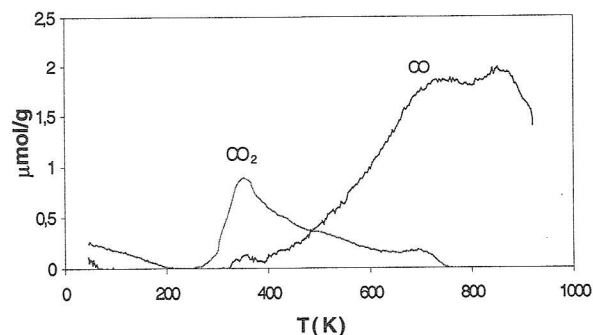


Fig.1. TPD for ACNa3

TPD curves for different activated carbons (ACNa1, ACNa2, ACNa3, ACNa4, ACNa6) have very similar shapes, so they have similar oxygen groups structure. Different activation agent to carbon ratio does not change structure and quantity of surface groups. The amounts of  $CO$  and  $CO_2$  released can be obtained by integration of the areas under the

TPD peaks. The amounts for carbon ACNa3 are: for the CO<sub>2</sub> 460,09 μmol/g, for the CO 1942,22 μmol/g. These amounts are quantitative characteristics of the surface chemistry. High amount of the CO is usual for the chemical activation methods used.

It is established in literature that CO<sub>2</sub> peak results from carboxylic acid at low temperatures, or lactones at higher temperatures, carboxylic anhydrides originate both CO and CO<sub>2</sub> peak; phenols, ethers, and carbonyls originate a CO peak [10,11].

Characterization of the porous texture of the activated carbon can be examined after the adsorption of N<sub>2</sub> at 77K and CO<sub>2</sub> adsorption at 273K. The advantage of N<sub>2</sub> adsorption is that it covers relative pressures from 10<sup>-8</sup> to 1, which results in the whole range of porosity. The main disadvantage of N<sub>2</sub> adsorption at 77K is that when it is used for the characterization of microporous solids, diffusional problems of the molecules inside the narrow porosity range (<0,7nm) occur. In case of CO<sub>2</sub> adsorption, though the critical dimension of the CO<sub>2</sub> is similar to that of N<sub>2</sub>, the higher temperature of adsorption used for CO<sub>2</sub> results in a larger kinetic energy of the molecules able to enter into the narrow porosity [12].

The N<sub>2</sub> adsorption isotherm for carbon ACNa3 is presented in Fig. 2. and CO<sub>2</sub> adsorption isotherm is presented in Fig. 3.

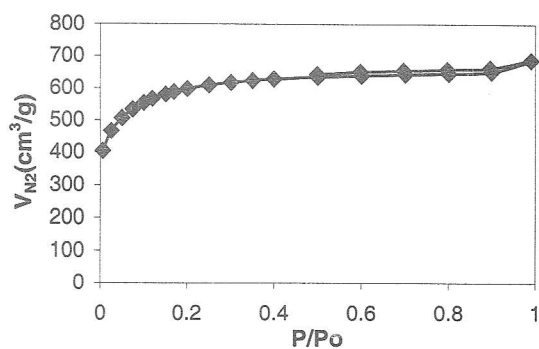


Fig. 2. N<sub>2</sub> adsorption isotherm for ACNa3

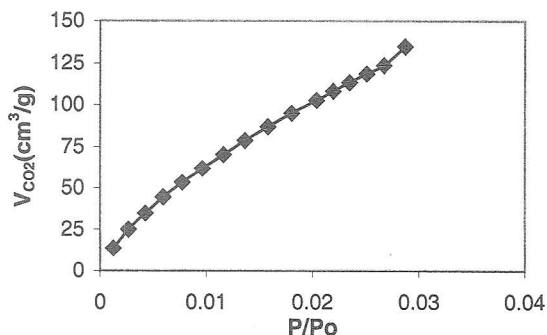


Fig. 3. CO<sub>2</sub> adsorption isotherm for ACNa3

Desorption of N<sub>2</sub> was done just after adsorption (shorter curve in Fig. 2. is related to desorption). It can be clearly seen from the Fig. 2. that desorption curve is similar to adsorption one. The N<sub>2</sub> adsorption isotherm is of type I in the Brunauer, Deming, Deming and Teller (BDDT)

classification. That type is common for the microporous materials [13,14].

The micropore volume can be calculated applying Dubinin-Radushkevich (DR) equation:

$$\frac{V}{V_0} = \exp\left(-\frac{K}{\beta^2} \left(RT \ln \frac{P_0}{P}\right)^2\right) \quad (1)$$

where  $V$  is volume adsorbed at pressure  $P$ ,  $V_0$  is the micropore value,  $K$  is a constant dependent on the pore structure, and  $\beta$  is affinity coefficient that is characteristic of the adsorptive [12].

Micropore volumes and surface areas for the N<sub>2</sub> and CO<sub>2</sub> adsorbed were calculated applying DR equation (Table 1.).

Table 1. Micropore volumes and surface areas for activated carbons (N<sub>2</sub> and CO<sub>2</sub> adsorption)

Carbon	V <sub>N2</sub> (cm <sup>3</sup> /g)	S <sub>N2</sub> (m <sup>2</sup> /g)	V <sub>CO2</sub> (cm <sup>3</sup> /g)	S <sub>CO2</sub> (m <sup>2</sup> /g)
ACNa1	0.45	1267.2	0.46	1204.6
ACNa2	0.64	1802.2	0.65	1702.1
ACNa3	0.95	2671.9	0.65	1702.1
ACNa4	0.54	1520.6	0.53	1387.9
ACNa6	0.55	1548.7	0.60	1571.2

From the calculated values it can be observed that when NaOH/coal ratio increases up to a value of 3, the micropore value and the surface area increase. Above this value, the effect of NaOH/coal ratio is much less marked.

Chemical activation by NaOH permits to develop a rather homogeneous narrow microporosity. When micropore volumes for N<sub>2</sub> adsorption is similar to volume for CO<sub>2</sub> adsorption carbon has homogeneous narrow microporosity. When the NaOH/coal ratios are 1/1, 2/1 and 6/1 the micropore volume for CO<sub>2</sub> adsorption is higher then when N<sub>2</sub> is used. For a ratio 3/1 the micropore value for N<sub>2</sub> is higher, which means that contribution of narrow micropores is lower.

The optimum maximum temperature of around 700°C, and heating rate of 5°C/min. have been established in literature. Also, higher N<sub>2</sub> flow rates were suggested for well developed microporosity [6].

Chemical activation involving KOH as an activated agent renders similar results. For example when KOH/coal ratio is 2, the micropore volume is 0.89 cm<sup>3</sup>/g for N<sub>2</sub> adsorption and 0.86 cm<sup>3</sup>/g for CO<sub>2</sub>. When ratio is 3 volume is 1.35 cm<sup>3</sup>/g for N<sub>2</sub> adsorption and 0.81 cm<sup>3</sup>/g for CO<sub>2</sub>. For KOH/coal ratio 4 the micropore volume is 1.45 cm<sup>3</sup>/g for N<sub>2</sub> and 0.81 cm<sup>3</sup>/g for CO<sub>2</sub> adsorption [6]. These results show that KOH activation develops activated carbons with higher micropore volumes. But, preparation method for NaOH activation was physical mixing which is much simpler then conventional impregnation process used for KOH activation.

The micropore volumes of activated carbons synthesised through physical activation are much lower then those prepared using chemical activation. For example, when activating agent was CO<sub>2</sub> micropore volumes for N<sub>2</sub> adsorption were from 0.25 up to 0.49 cm<sup>3</sup>/g, and volumes for CO<sub>2</sub> adsorption were from 0.26 up to 0.34 cm<sup>3</sup>/g [4]. When activating agent in physical activation was combination of

steam and CO<sub>2</sub>, micropore volumes for N<sub>2</sub> adsorption were from 0.25 up to 0.7 cm<sup>3</sup>/g, and volumes for CO<sub>2</sub> were from 0.21 up to 0.4 cm<sup>3</sup>/g (mostly around 0.3 cm<sup>3</sup>/g) [5]. These volumes show that chemical activation renders better results, producing activated carbons with well developed narrow micropore structure. Moreover, chemical activation method is much simpler than the physical one.

#### 4. CONCLUSIONS

Chemical activation of a Spanish anthracite with sodium hydroxide is a suitable method for preparing activated carbons highly microporous. Sodium hydroxide is cheaper and less corrosive than the typical activating agents used. The physical mixing of NaOH and coal is a very easy method that simplifies the first step of the preparation. The best development of porosity can be achieved with activating agent to carbon ratio of three.

#### 5. REFERENCES

- [1] R.C. Bansal, J.B. Donnet and F. Stoeckli, "Active Carbon", New York : Marcel Dekker, 1988.
- [2] Roskill, "The Economics of Activated Carbon", London : Roskill Information Services, Ltd., 1990.
- [3] H. Jankowska, A. Swiatkowski and J. Choma, "Active Carbon", London : Ellis Horwood, 1991.
- [4] M.J. Munoz-Guillena, M.J. Illan-Gomez, J.M. Martin-Martinez, A. Linares-Solano and C. Salinas-Martinez de Lecea, "Activated Carbons from Spanish Coals. 1. Two-Stage CO<sub>2</sub> Activation", *Energy & Fuels*, 6, pp. 6-15, 1992.
- [5] F. Rodriguez-Reinoso, M. Molina-Sabio and M.T. Gonzales, "The Use of Steam and CO<sub>2</sub> as Activating Agents in the Preparation of Activated Carbons", *Carbon*, 33, pp. 15-23, 1995.
- [6] D. Lozano-Castello, M.A. Lillo-Rodenas, D. Cazorla-Amoros and A. Linares-Solano, "Preparation of activated carbons from Spanish anthracite - I. Activation by KOH", *Carbon*, 39, pp. 741-749, 2001.
- [7] M. Molina-Sabio, F. Rodríguez-Reinoso, F. Caturla and M. J. Selles, "Porosity in granular carbons activated with phosphoric acid", *Carbon*, 33 pp. 1105-1113, 1995.
- [8] M. Molina-Sabio, F. Rodriguez-Reinoso, F. Caturla and M. J. Selles, "Development of porosity in combined phosphoric acid-carbon dioxide activation", *Carbon*, 34, pp. 457-462, 1996.
- [9] M.J. Illan-Gomes, A. Garcia-Garcia, C. Salinas-Martinez de Lecea and A. Linares-Solano, "Activated Carbons from Spanish Coals. 2. Chemical Activation", *Energy & Fuels*, 10, pp.1108-1114, 1996.
- [10] J.L. Figueiredo, M.F.R. Pereira and J.J.M. Orfao, "Modification of the Surface Chemistry of Activated Carbons", *Carbon*, 37, pp.1379-1389, 1999.
- [11] H.P. Boehm, "Surface Oxides on Carbon", *High Temp.-High Press.*, 22, 1990.
- [12] D. Cazorla-Amoros, J. Alcaniz-Monge, A. Linares-Solano, "Characterization of activated Carbon Fibers by CO<sub>2</sub> Adsorption", *Langmuir*, 12, pp. 2820-2824, 1996.
- [13] A. Gil, "Analysis of the Micropore Structure of Various Microporous Materials from Nitrogen Adsorption at 77K", *Adsorption*, 4, pp. 197-206, 1998.
- [14] S.J. Gregg, K.S.W. Sing, "Adsorption, Surface Area and Porosity", *Academic Press, London*, 1991.



## INSTRUCTION FOR AUTHORS

*Name of the author/s, Affiliation/s*

**Abstract:** Short instruction for authors is presented in this paper. Works that are to be printed in the review "Electronics" should be typed according to this instruction.

**Keywords:** Review Electronics, Faculty of Electrical Engineering in Banjaluka, Instruction for authors.

### 1. INTRODUCTION

In the review "Electronics", we publish the scientific and professional works from different fields of electronics in the broadest sense like: automatics, telecommunications, computer techniques, power engineering, nuclear and medical electronics, analysis and synthesis of electronic circuits and systems, new technologies and materials in electronics etc. In addition to the scientific and professional works, we present new products, new books, B. Sc., M. Sc. and Ph.D. theses.

In order to enable the unification of the technical arrangement of the works, to simplify the printing of the review "ELECTRONICS", we are giving this instruction for the authors of the works to be published in this professional paper.

### 2. TECHNICAL DETAILS

#### 2.1. Submitting the papers

The works are to be delivered to the editor of the review by the E-mail (elektronika@etfbl.net) or on floppy (or CD) by post mail to the address of the Faculty of Electrical Engineering (Elektrotehnicki fakultet, Patre 5, 78000 Banja Luka, Republic of Srpska, Bosnia and Herzegovina).

#### 2.2. Typing details

The work has to be typed on the paper A4 format, 8.27" width and 11.69" height (21.0x29.7 cm), upper and lower margins of 1" (2.54 cm), left and right margins of 1" (2.54 cm) and the header and footer are 0,5" (1.27cm). The work has to be written in English language. Our suggestion to the authors is to make their works on a PC using the word processor MS WORD 97/2000, and for the figures to use the graphic program CorelDraw, if the graphs are not going from the original programs, i.e., from the programs received (like MATLAB).

The title of the work shall be written on the first page, in bold and 12 pt. size. Also, on the first page, moved for one line spacing from title, the author's name together with the name of his institution shall be printed in the letter size (10pt, *Italic*). The remaining parts of the manuscript shall be done in two columns with 0.5cm distance. The work shall be typed with line spacing 1 (Single) and size not less than 10 pt (like as this instruction). After the title of the work and the name of the author/s, a short content in English language follows, written in italics. The subtitles in the text shall be written in bold, capital letters of the size as in the text (not less than 10 pt.). Each work shall, at the beginning, comprise a subtitle INTRODUCTION, and, at the end, the subtitles CONCLUSION and BIBLIOGRAPHY / REFERENCES.

The operators and size marks that do not use numerical values, shall be written in common letters. The size marks that can use numerical values shall be written in italics. The equations shall be written in one column with right edge numeration. If the breaking of equations or figures is desired, those may be placed over both columns.

Illustrations (tables, figures, graphs etc.) may be wider than one column if necessary. Above a table there shall be a title, for instance: Table 2. *The experimental measuring results*. The same applies to figures and graphs but the accompanying text comes underneath the figure of graphs, for instance: Fig.3: *Equivalent circuit diagram...*

The work should not be finished at the beginning of a page. If the last manuscript page is not full, the columns on that page should be made even. Number of pages should not go over 6.

### 3. CONCLUSION

This short instruction is presented in order to enable the unification of technical arrangement of the works.

### 4. REFERENCES

At the end of work, the used literature shall be listed in order as used in the text. The literature in the text, shall be enclosed in square brackets, for instance: ...in [2] is shown ...

## ELECTRONICS

Vol. 6, No. 1, December 2002.

### CONTENTS

<b>PREFACE</b> .....	1
<b>BIOGRAPHIES OF GUEST EDITORS</b> .....	2
<b>DESIGN OF PRINTED CIRCUIT BOARDS FOR LOW POWER RADIO TRANSMITTERS</b> .....	3
Miljana Sokolović, Dragiša Milovanović	
<b>A CONCEATENATIVE TTS SYSTEM IN SERBIAN LANGUAGE BASED ON REAL-TIME SELECTION OF SEGMENTS</b> .....	7
Milan Sečujski, Radovan Obradović, Darko Pekar, Ljubomir Jovanov	
<b>INFLUENCE OF LOADED WAGON ON ELECTROMAGNETIC FIELD DISTRIBUTION IN MINE PIT</b> .....	11
Dijana G. Zulkić, Saša S. Ilić	
<b>ANALYSIS OF NEURAL NETWORK MODELS OF SERBIAN SPEECH CONSONANTS</b> .....	15
Danijela Arsenijević, Milan M. Milosavljević	
<b>A NOVEL DIRECT TORQUE CONTROL APPROACH IN INDUCTION MACHINE DRIVES</b> .....	18
Petar Matić, Branko Blanuša, Slobodan Vukosavić	
<b>A POSSIBILITY OF DIGITAL IMAGE COMPRESSION BASED ON CONDITIONAL PROBABILITIES</b> .....	22
Đ. Đurđević, D. Dujković, M. Potrebić	
<b>A SWITCHING SOURCE OF ARTIFICIAL ELECTROMAGNETIC</b> .....	26
Milan Ponjavić, Radivoje Đurić, Nenad Smiljanić	
<b>CURRENT GAIN FREQUENCY CHARACTERISTICS OF ULTRA – NARROW BASE BIPOLAR TRANSISTORS</b> .....	30
Tatjana Pešić, Nebojša Janković, Jugoslav Karamaković	
<b>ACTIVE MICROWAVE MULTIPLIERS AT X BAND</b> .....	33
Darko Radulović, Aleksandar Nešić	
<b>PREPARATION OF ACTIVATED CARBONS BY NAOH</b> .....	37
Nikola Nikačević, Encarnacion Raymundo – Pinero	